

Radiometric force on a sphere in a rarefied gas flow based on the Cercignani-Lampis model of gas-surface interaction.

Denize Kalempa^a, Felix Sharipov^b

^a*Departamento de Ciências Básicas e Ambientais, Escola de Engenharia de Lorena, Universidade de São Paulo, 12602-810, Lorena, Brazil*

^b*Departamento de Física, Universidade Federal do Paraná, Caixa Postal 19044, 81531-990, Curitiba, Brazil*

Abstract

The radiometric force on a sphere due to its thermal polarization in a rarefied gas flow being in equilibrium is investigated on the basis of a kinetic model to the linearized Boltzmann equation. The scattering kernel proposed by Cercignani and Lampis to model the gas-surface interaction using two accommodation coefficients, namely the tangential momentum accommodation coefficient and the normal energy accommodation coefficient, is employed as the boundary condition. The radiometric force on the sphere, as well as the flow field of the gas around it, are calculated in a wide range of the gas rarefaction, defined as the ratio of the sphere radius to an equivalent free path of gaseous particles, covering the free molecular, transition and continuum regimes. The discrete velocity method is employed to solve the kinetic equation numerically. The calculations are carried out for values of accommodation coefficients considering most situations encountered in practice. To confirm the reliability of the calculations, the reciprocity relation between the cross phenomena is verified numerically within a numerical error of 0.1%. The temperature drop between two diametrically opposite points of the spherical surface in the direction of the gas flow stream, which characterizes the thermal polarization effect, is compared to experimental data for a spherical particle of Pyrex glass immersed in helium and argon gases.

Keywords: Radiometric force, viscous drag, kinetic equation, Cercignani-Lampis scattering kernel, thermal polarization.

1. Introduction

In the framework of rarefied gas dynamics, it is well known that a steady gas flow can be induced by a temperature field in the absence of external forces such as gravity, e.g. the thermal creep flow in the vicinity of a boundary with a longitudinal temperature distribution [1–4]. Nonetheless, the gas motion can also induce a thermal effect, e.g. the thermal polarization of a body in a uniform gas flow [5, 6] which leads to the so called radiometric force on the body. The nonequilibrium phenomena arising within the Knudsen layer are peculiar to rarefied gases and cannot be predicted by the classical equations of fluid mechanics [7]. The Knudsen number, Kn , defined as the ratio of the molecular mean free path to a characteristic length scale of the gas flow, is the parameter used to classify the gas flow regime as free molecular ($Kn \gg 1$), transitional ($Kn \sim 1$) and continuum ($Kn \ll 1$). For instance, in problems concerning the transport of small particles in a rarefied gas, such as air at the standard conditions where the molecular mean free path is approximately $0.065 \mu\text{m}$, the Knudsen number varies from approximately zero to 65 when the size of particles ranges from $100 \mu\text{m}$ to $10^{-3} \mu\text{m}$. Therefore, the equations of continuum mechanics are not valid to describe the gas flow around aerosols in the atmosphere as well as in many applications which rely on aerosols dynamics. Moreover, even in the continuum regime there are phenomena which cannot be predicted by the Navier-Stokes-Fourier equations, e.g. the negative thermophoresis in aerosols with a high thermal conductivity related to that of the carrier gas. The negative thermophoresis was first predicted theoretically by Sone [8] as a result of the thermal stress slip flow, which is an effect of second order in the Knudsen number. Experimentally, the negative thermophoresis was already detected, see e.g. Ref. [9], in which the thermophoretic force on a copper sphere in argon gas was measured in a wide range of the Knudsen number. The radiometric force which appears in a body placed in an equilibrium gas is also an effect of second order in the Knudsen number and it is not predicted by the classical equations of continuum mechanics. Although the magnitude of the radiometric force on a particle in a uniform gas flow is negligible compared to the viscous drag force, this force plays an important role in thermophoresis of particles with arbitrary thermal conductivity. Thus, problems concerning the movement of small particles in rarefied gases must be solved at the microscopic level by employing the methods of rarefied gas dynamics, which are based on the solution of the Boltzmann equation [10, 11] and its related kinetic models, such as the models proposed by Bhatnagar, Gross and Krook [12] and Shakhov [13], or on the direct simulation Monte Carlo method [14].

Historically, the term radiometric force is widely known from the experi-

ments designed by Crookes in the 19th century concerning the rotation of a windmill in a closed vessel by the incidence of light [15]. Since the Crooke's theory of pressure radiation was not successful to provide an overall explanation for the physics underlying his experiments, other theories were proposed over the years by prominent scientists such as Reynolds, Maxwell and Einstein, see e.g. Refs. [16, 17]. However, the more reasonable explanation for the origin of the force in the Crookes radiometer were those proposed by Maxwell [18] and Reynolds [19] which rely on kinetic theory of gases [1]. A more recent historical review on radiometric phenomena, including some applications, is given in Ref. [20]. It is worth mentioning that the increasing interest in numerical and experimental studies concerning the radiometric force is due to the promising applications in the field of micro and nano technology, see e.g. the literature review on Knudsen pumps [21] and Refs. [22, 23] concerning gas sensors. The description of the main mechanisms of thermally induced flows which lead to the radiometric force in rarefied gas systems is given in Ref. [24]. It is important to point out that there are many possibilities to build a configuration in which the radiometric force arises. In thin plates it is usually called Knudsen force due to the pioneering works by Knudsen, e.g. Ref. [25]. Small particles in a rarefied gas illuminated by a beam of light or other radiation also experience a radiometric force as well as a radiation pressure force. In this case, the non-uniform heating of particles is caused by the absorption of electromagnetic energy and the force is called as photophoretic. Thus, studies concerning radiometric phenomena in rarefied gases are also important to understand the physics underlying the transport of aerosols in the atmosphere due to absorption of solar radiation and in applications such as the optical trapping and manipulation of small particles [26]. According to Ref. [26], in a gas medium the photophoretic force dominates the optical manipulation of light-absorbing particles because its order of magnitude is larger than that corresponding to the pressure-radiation.

Usually, the classical problem of viscous drag on a sphere relies on the assumption of uniform temperature on the spherical surface, which is valid in case of a sphere with high thermal conductivity related to that of the carrier gas. Otherwise, for low and moderate thermal conductivity of the solid particle, the non-uniform temperature of its surface due to the thermal polarization in a uniform gas flow must be considered in the boundary condition. The temperature non-uniformity of the spherical particle leads to nonequilibrium phenomena in the vicinity of the boundary from which arise the radiometric force on the sphere. This force as well as the macroscopic characteristics of the gas flow around the sphere induced by the temperature field are strongly dependent on the gas-surface interaction law and accommodation coefficients at the spherical surface. In fact, experiments on thermal

polarization of small particles can be carried out to determine the values of the accommodation coefficients, see e.g. Ref. [6]. Thus, the proper modelling of the gas flow around the sphere and the calculation of the force acting on it depends on the mathematical model of gas-surface interaction and correct values of accommodation coefficients. Currently, there are few papers in the literature concerning the influence of the gas-surface interaction law on the radiometric phenomenon in the whole range of the gas rarefaction and most of them are restricted to the assumption of diffuse scattering or complete accommodation of gas molecules on the surface. To the best of our knowledge, Beresnev and coworkers [27] were the first authors to analyse the influence of the accommodation coefficients on the radiometric force on a sphere in a uniform gas flow by solving a kinetic model to the Boltzmann equation in the whole range of the Knudsen number. As pointed out in our previous work [28], in the boundary condition used in Ref. [27], the distribution function of reflected molecules was expanded in Hermite polynomials and the unknown accommodation coefficients of momentum and energy were determined from the conservation laws of momentum and energy on the surface. Moreover, the variational method was applied by the authors to solve the kinetic equation. The results presented in Ref. [27] for the temperature difference between the two diametrically opposite points of the spherical surface in the direction of the gas flow stream, which characterizes the thermal polarization, showed a strong dependence on the accommodation coefficients.

An interesting feature of rarefied gas flows induced by temperature fields is the absence of gas motion in the free molecular regime when the diffuse-specular model of gas-surface interaction proposed by Maxwell [29] is used in the boundary condition, see e.g. Refs. [30–32]. The model proposed by Maxwell assumes that only a part of the gas molecules is reflected diffusely, while the remaining part is reflected specularly. In spite of widely used due to its mathematical simplicity, the Maxwell model has some drawbacks. For instance, the Maxwell model cannot predict the correct exponent which appears in the thermomolecular pressure difference (TPD) in the free molecular regime. For instance, while many experiments lead to an TPD exponent varying from 0.4 to 0.5, see e.g. Refs. [34, 35], the Maxwell model always provides a value of 0.5. To verify if a steady gas flow is induced by a temperature field in the free molecular regime when other model of gas-surface interaction is used, Kosuge *et al.* [36] carried out the calculations for the problem of a rarefied gas between parallel plates with non-uniform temperature by employing the model of gas-surface interaction proposed by Cercignani and Lampis (CL) [37]. In spite of the mathematical complexity, the CL model of gas-surface interaction allows the setting of two accommodation coefficients, namely the tangential momentum accommodation coefficient (TMAC) and

the normal energy accommodation coefficient (NEAC). Currently, the values of the NEAC and TMAC extracted from experiments can be found in the literature for several gases and surfaces, see e.g. [38–41]. For instance, the NEAC ranges from 0 to 0.1 for helium and from 0.5 to 0.95 for argon at ambient temperature and metallic surfaces such as aluminum, platinum and stainless steel, while the TMAC ranges from 0.5 to 0.95 for both gases at the same conditions. According to the results presented in Ref. [36], obtained by applying a deterministic method to solve the integral equation derived from the Boltzmann equation in the free molecular limit, a steady gas flow is induced by the temperature field in case of non-difuse scattering of gas molecules on the surface. In fact, different gas flow patterns were observed between the plates by varying the accommodation coefficients.

In our previous paper [28], the CL model of gas-surface interaction was employed in the modelling of the viscous drag and thermophoresis on a sphere in a rarefied gas. The case of particle with high thermal conductivity related to that of the carrier gas was considered so that the temperature of the sphere was assumed as being a constant. The modelling was based on the numerical solution of the Shakhov model [13] for the linearized Boltzmann equation via the discrete velocity method. The drag and thermophoretic forces on the sphere, as well as the flow fields around it, were obtained in a wide range of the Knudsen number and accommodation coefficients. According to the previous results, both forces are sensitive to the accommodation coefficients. Indeed, for some sets of accommodation coefficients, the appearance of the negative thermophoresis was observed in the near continuum regime.

In the present work, the problem of radiometric force on a spherical particle caused by its thermal polarization in a uniform gas flow is investigated numerically with basis on the kinetic model proposed by Shakhov [13] for the linearized Boltzmann equation and the discrete velocity method. As already mentioned, the magnitude of this force is negligible compared to the viscous drag force, but it plays an important role in thermophoresis of particles immersed in a rarefied gas. It is worth mentioning that nowadays, in spite of the great computational infrastructure available, the kinetic models are still widely used because their solutions require a modest computational effort compared to that required to solve the exact Boltzmann equation. The kinetic model proposed by Shakhov is considered the most reliable to deal with problems concerning both heat and mass transfer in a single gas because it provides the correct Prandtl number, i.e. the correct values for the viscosity and heat conductivity of the gas, and maintains the original properties of the Boltzmann equation corresponding to mass, momentum and energy conservation laws, and the H-theorem. Moreover, it provides a good accuracy and its reliability is supported by the literature. For instance, for the

classical problems of Couette flow and heat transfer between parallel plates, the comparison between the results obtained from the Shakhov model and those obtained from the Boltzmann equation for hard-spheres potential is presented in Refs. [11, 43, 44] and shows that the difference is within 5%. In the context of forces on small particles in a rarefied gas, a similar comparison is presented in Refs. [27, 28, 45] and shows that the difference is within 5-7%. The calculations are carried out in a range of the Knudsen number which covers the free molecular, transition and continuum regimes. Moreover, a wide range of the NEAC and TMAC is considered. The fulfillment of the reciprocity relation between cross phenomena is verified. As results, the radiometric force on the sphere and the flow fields around it induced by the temperature field are presented. The temperature drop between the two diametrically opposite points in the sphere in the direction of the gas flow stream is calculated and the results are compared to the experimental data provided in Ref. [6] for a Pyrex glass sphere immersed in helium and argon gas.

2. Statement of the problem

Let us consider a sphere of radius R_0 and thermal conductivity λ_p at rest placed in a monoatomic rarefied gas of thermal conductivity λ_g . Far from the sphere, the gas flows with a constant bulk velocity U_∞ in the z' -direction as showed in Figure 1. Moreover, far from the sphere the equilibrium gas number density, temperature and pressure are denoted by n_0 , T_0 and p_0 , respectively, and these quantities are related by the state equation $p_0=n_0kT_0$, where k denotes the Boltzmann constant.

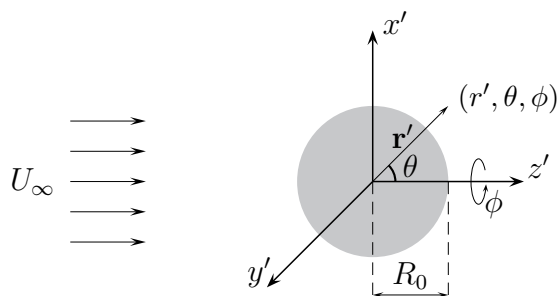


Figure 1: Scheme of the problem

Due to the geometry of the problem, spherical coordinates (r', θ, ϕ) in the physical space are introduced so that the components of the position vector

\mathbf{r}' of gaseous particles read

$$x' = r' \sin \theta \cos \phi, \quad (1a)$$

$$y' = r' \sin \theta \sin \phi, \quad (1b)$$

$$z' = r' \cos \theta. \quad (1c)$$

Moreover, the components of the molecular velocity vector \mathbf{v} are given as

$$v_x = (v_r \sin \theta + v_\theta \cos \theta) \cos \phi - v_\phi \sin \phi, \quad (2a)$$

$$v_y = (v_r \sin \theta + v_\theta \cos \theta) \sin \phi + v_\phi \cos \phi, \quad (2b)$$

$$v_z = v_r \cos \theta - v_\theta \sin \theta, \quad (2c)$$

where v_r , v_θ and v_ϕ are the radial, polar and azimuthal components of the molecular velocity vector, respectively, which are written in spherical coordinates (v, θ', ϕ') in the velocity space as follows

$$v_r = v \cos \theta', \quad (3a)$$

$$v_\theta = v_t \cos \phi', \quad (3b)$$

$$v_\phi = v_t \sin \phi', \quad (3c)$$

with the tangential component given as

$$v_t = \sqrt{v_\theta^2 + v_\phi^2} = v \sin \theta'. \quad (4)$$

For convenience, hereafter, the dimensionless sphere radius, r_0 , as well as the position \mathbf{r} and molecular velocity \mathbf{c} vectors are introduced as

$$r_0 = \frac{R_0}{\ell_0}, \quad \mathbf{r} = \frac{\mathbf{r}'}{\ell_0}, \quad \mathbf{c} = \frac{\mathbf{v}}{v_0}, \quad (5)$$

where ℓ_0 and v_0 denote the equivalent free path and the most probable molecular speed, defined as

$$\ell_0 = \frac{\mu_0 v_0}{p_0}, \quad v_0 = \sqrt{\frac{2kT_0}{m}}. \quad (6)$$

Here, μ_0 denotes the viscosity of the gas at temperature T_0 , while m is the molecular mass.

It is assumed that the ratio of thermal conductivities, $\Lambda = \lambda_p / \lambda_g$, is arbitrary. As a consequence, the non-uniform temperature of the spherical surface must be taken into account in the solution of the problem because it induces a gas flow around the sphere as well as a radiometric force on the

sphere. Thus, the temperature of the spherical particle, T_p , is obtained from the solution of the Laplace equation for heat conduction with axial symmetry written as

$$\left[\frac{\partial^2}{\partial r^2} + \frac{2}{r} \frac{\partial}{\partial r} + \frac{1}{r^2 \sin \theta} \frac{\partial}{\partial \theta} \left(\sin \theta \frac{\partial}{\partial \theta} \right) \right] T_p(r, \theta) = 0. \quad (7)$$

The solution of equation (7) must satisfy two conditions. Firstly, the continuity of the radial component of the heat flux at the gas-solid interface which reads

$$q_r(r_0, \theta) = -\frac{15}{8} \frac{\Lambda}{T_0} \frac{\partial T_p}{\partial r}, \quad (8)$$

where the dimensionless radial component of the heat flux was introduced as

$$q_r = \frac{Q_r}{p_0 v_0}, \quad (9)$$

with Q_r denoting the corresponding dimensional quantity. Secondly, the condition of finite temperature at the center of the spherical particle, i.e. at $r=0$, must be satisfied. Thus, the solution of the heat conduction equation (7) satisfying both conditions leads to the following temperature distribution at the spherical surface of the solid particle

$$T_p(r_0, \theta) = T_0(1 + \tau_{s0} \cos \theta), \quad (10)$$

where τ_{s0} is a constant which depends on the gas flow stream and heat conductivity of the particle. Note that the same temperature distribution on the particle surface can be caused by a light radiation. In this case, τ_{s0} depends on the light intensity and heat conductivity of the particle. Thus, the solution presented below is determined by the distribution (10), but it is independent of the physical phenomenon leading to the distribution.

Two dimensionless thermodynamic forces are introduced as

$$X_u = \frac{U_\infty}{v_0}, \quad X_q = \tau_{s0}. \quad (11)$$

It is assumed a weak disturbance from thermodynamic equilibrium, which means

$$|X_u| \ll 1, \quad |X_q| \ll 1. \quad (12)$$

The thermodynamic forces are coupled due to the effect of thermal polarization of the particle in the moving gas. However, the assumptions given

in (12) allow us to decompose the problem into two independent parts corresponding to viscous drag on a sphere with uniform temperature and radiometric force on a sphere with non-uniform temperature placed in an equilibrium gas. Thus, after solving the problem separately for each thermodynamic force, a solution describing the real situation is given as a superposition of the obtained solutions. Note that the radial heat flux $q_r(r_0, \theta)$, given in (8), accounts to the isothermal heat transfer due to the gas motion as well as to the non-isothermal heat transfer due to the temperature difference between the particle and the gas around it.

The main parameter determining the solution of the problem is the rarefaction parameter, δ , which is inversely proportional to the Knudsen number, but defined here as the ratio of the sphere radius to the equivalent molecular free path, i.e.

$$\delta = \frac{R_0}{\ell_0}, \quad (13)$$

where ℓ_0 is defined in (6). Note that, according to (5), $r_0 = \delta$. When $\delta \ll 1$ the gas is in the free molecular regime, while the opposite limit, $\delta \gg 1$, corresponds to the continuum or hydrodynamic regime. In other situations, $\delta \sim 1$, the gas is in the transition regime.

The CL-model of the gas-surface interaction [37] is employed in the boundary condition. In this model, the type of the gas-surface interaction is chosen by setting appropriate values for the NEAC and TMAC. Henceforth, these accommodation coefficients will be denoted by α_n and α_t , respectively. The widely used diffuse scattering or complete accommodation on the surface corresponds to $\alpha_n = 1$ and $\alpha_t = 1$.

The influence of the NEAC and TMAC on the viscous drag on a sphere with high thermal conductivity related to that of the carrier gas, which corresponds to the case of a sphere with uniform temperature, was already investigated in our previous work [28] in a range of the gas rarefaction which covers the free molecular, transition and hydrodynamic regimes. Thus, in the present work, focus is given to the solution due to the thermodynamic force X_q . We are going to calculate the radiometric force on the sphere and the flow fields around it induced by X_q in a wide range of the gas rarefaction and accommodation coefficients. It is worth mentioning that the radiometric force is negligible compared to the viscous drag force on the sphere, but the introduction of two thermodynamic forces as defined in (11) allows us to verify the fulfillment of the reciprocity relation between cross phenomena as an additional criterium for the accuracy of the numerical calculations.

3. Kinetic equation

Similarly to our previous work [28], the model proposed by Shakhov [13] for the Boltzmann equation is employed here due to its reliability to deal with problems concerning both mass and heat transfer. Thus, the kinetic equation is written as

$$\mathbf{v} \cdot \frac{\partial f}{\partial \mathbf{r}'} = Q(ff_*), \quad (14)$$

where $f=f(\mathbf{r}', \mathbf{v})$ is the distribution function of molecular velocities and

$$Q(ff_*) = \nu_S \left\{ f^M \left[1 + \frac{4}{15} \left(\frac{V^2}{v_0^2} - \frac{5}{2} \right) \frac{\mathbf{Q} \cdot \mathbf{V}}{p_0 v_0^2} \right] - f(\mathbf{r}', \mathbf{v}) \right\} \quad (15)$$

is the intermolecular collision integral. The local Maxwellian function reads

$$f^M(\mathbf{r}', \mathbf{v}) = n \left[\frac{m}{2\pi kT(\mathbf{r}')} \right]^{3/2} \exp \left[-\frac{m\mathbf{V}^2}{2kT(\mathbf{r}')} \right], \quad (16)$$

the quantity ν_S has the order of the intermolecular interaction frequency and $\mathbf{V}=\mathbf{v} - \mathbf{U}$ is the peculiar velocity so that $V = |\mathbf{V}|$ denotes its magnitude. $\mathbf{U}(\mathbf{r}')$ and $\mathbf{Q}(\mathbf{r}')$ are the bulk velocity and heat flux vectors.

The assumptions of smallness of the thermodynamic forces X_u and X_q , defined in (11), allow us to linearize the kinetic equation by representing the distribution function of molecular velocities as

$$f(\mathbf{r}, \mathbf{c}) = f_R^M [1 + h^{(u)}(\mathbf{r}, \mathbf{v})X_u + h^{(q)}(\mathbf{r}, \mathbf{v})X_q], \quad (17)$$

where $h^{(u)}$ and $h^{(q)}$ are the perturbation functions due to the thermodynamic forces X_u and X_q , respectively. The reference Maxwellian function is given by the equilibrium distribution function far from the sphere, i.e.

$$f_R^M = f_\infty^M = f_0 (1 + 2c_z X_u), \quad (18)$$

where f_0 is the global Maxwellian function.

The representation (17) allows to write the gas number density, the temperature, the dimensionless bulk velocity and heat flux vectors as follows

$$n(r, \theta) = n_0 [1 + \nu^{(u)}(r, \theta)X_u + \nu^{(q)}(r, \theta)X_q], \quad (19)$$

$$T(r, \theta) = T_0 [1 + \tau^{(u)}(r, \theta)X_u + \tau^{(q)}(r, \theta)X_q], \quad (20)$$

$$\mathbf{u}(r, \theta) = \frac{\mathbf{U}}{v_0} = \mathbf{u}^{(u)}(r, \theta)X_u + \mathbf{u}^{(q)}(r, \theta)X_q, \quad (21)$$

$$\mathbf{q}(r, \theta) = \frac{\mathbf{Q}}{p_0 v_0} = \mathbf{q}^{(u)}(r, \theta)X_u + \mathbf{q}^{(q)}(r, \theta)X_q, \quad (22)$$

where $\nu^{(n)}$ and $\tau^{(n)}$ are the density and temperature deviations from equilibrium, while $\mathbf{u}^{(n)}$ and $\mathbf{q}^{(n)}$ are the bulk velocity and heat flux due to the corresponding thermodynamic force ($n=u, q$).

Thus, after substituting the representation (17), the dimensionless quantities defined in (5) and the macroscopic quantities (19)-(22) into (14), the linearized kinetic equation for each thermodynamic force is written as

$$\hat{D}h^{(n)} = \hat{L}_S h^{(n)}, \quad n = u, q. \quad (23)$$

Due to the spherical geometry of the problem, the kinetic equation (23) is written in spherical coordinates (r, θ, ϕ) in the physical space as well as in the molecular velocity space (c, θ', ϕ') . Details regarding this transformation can be found in Ref. [46]. Thus, after taking into account the symmetry of the problem on the azimuthal angle ϕ , the transport operator \hat{D} and the linearized collision integral \hat{L}_S appearing in the kinetic equation (23) are written as

$$\hat{D}h^{(n)} = c_r \frac{\partial h^{(n)}}{\partial r} - \frac{c_t}{r} \frac{\partial h^{(n)}}{\partial \theta'} + \frac{c_t}{r} \cos \phi' \frac{\partial h^{(n)}}{\partial \theta} - \frac{c_t}{r} \sin \phi' \cot \theta \frac{\partial h^{(n)}}{\partial \phi'} \quad (24)$$

and

$$\hat{L}_S h^{(n)} = \nu^{(n)} + \left(c^2 - \frac{3}{2}\right) \tau^{(n)} + 2\mathbf{c} \cdot \mathbf{u}^{(n)} + \frac{4}{15} \left(c^2 - \frac{5}{2}\right) \mathbf{c} \cdot \mathbf{q}^{(n)} - h^{(n)}, \quad (25)$$

where $h^{(n)} = h^{(n)}(r, \theta, \mathbf{c})$.

The macroscopic characteristics (19)-(22) are calculated as moments of the distribution function of molecular velocities and details concerning such a calculation can be found in Ref. [47]. In our notation, the density and temperature deviations from equilibrium read

$$\nu^{(n)}(r, \theta) = \frac{1}{\pi^{3/2}} \int h^{(n)}(r, \theta, \mathbf{c}) e^{-c^2} d\mathbf{c}, \quad (26)$$

$$\tau^{(n)}(r, \theta) = \frac{2}{3\pi^{3/2}} \int \left(c^2 - \frac{3}{2}\right) h^{(n)}(r, \theta, \mathbf{c}) e^{-c^2} d\mathbf{c}, \quad (27)$$

while the radial and polar components of the bulk velocity and heat flux vectors are given as

$$u_r^{(n)}(r, \theta) = \frac{1}{\pi^{3/2}} \int c_r h^{(n)}(r, \theta, \mathbf{c}) e^{-c^2} d\mathbf{c}, \quad (28)$$

$$u_\theta^{(n)}(r, \theta) = \frac{1}{\pi^{3/2}} \int c_\theta h^{(n)}(r, \theta, \mathbf{c}) e^{-c^2} d\mathbf{c}, \quad (29)$$

$$q_r^{(n)}(r, \theta) = \frac{1}{\pi^{3/2}} \int c_r \left(c^2 - \frac{5}{2} \right) h^{(n)}(r, \theta, \mathbf{c}) e^{-c^2} d\mathbf{c}, \quad (30)$$

$$q_\theta^{(n)}(r, \theta) = \frac{1}{\pi^{3/2}} \int c_\theta \left(c^2 - \frac{5}{2} \right) h^{(n)}(r, \theta, \mathbf{c}) e^{-c^2} d\mathbf{c}, \quad (31)$$

where $d\mathbf{c} = c^2 \sin \theta' dc d\theta' d\phi'$. The force acting on the sphere in the z' -direction is calculated from the normal and tangential stress on the sphere, whose expressions can be found in Ref. [47]. Here, the dimensionless force in the z -direction is introduced as

$$F_z = \frac{F'_z}{4\pi R_0^2 p_0} = F_u X_u + F_q X_q, \quad (32)$$

where the viscous drag force F_u and the radiometric force F_q are given as

$$F_u = -\frac{1}{2\pi^{5/2}} \int_{\Sigma_w} d\Sigma_w \int c_r c_z e^{-c^2} [h^{(u)}(r_0, \theta, \mathbf{c}) + 2c_z] d\mathbf{c}, \quad (33)$$

$$F_q = -\frac{1}{2\pi^{5/2}} \int_{\Sigma_w} d\Sigma_w \int c_r c_z e^{-c^2} h^{(q)}(r_0, \theta, \mathbf{c}) d\mathbf{c}. \quad (34)$$

$d\Sigma_w = \sin \theta d\theta d\phi$ denotes a dimensionless area element in the spherical surface.

Far from the sphere ($r \rightarrow \infty$), the asymptotic behavior of the perturbation functions are obtained from the Chapman-Enskog solution for the linearized kinetic equation as

$$h_\infty^{(u)} = \lim_{r \rightarrow \infty} h^{(u)}(r, \theta, \mathbf{c}) = 0, \quad (35)$$

$$h_\infty^{(q)} = \lim_{r \rightarrow \infty} h^{(q)}(r, \theta, \mathbf{c}) = 0. \quad (36)$$

4. Boundary condition

The boundary condition to solve the kinetic equation for each thermodynamic force is obtained from the relation between the distribution functions of incident particles on the sphere and reflected particles from the sphere. According to Refs. [10, 11], the general form of the linearized boundary condition at the spherical surface reads

$$h^{+(n)} = \hat{A}h^{-(n)} + h_w^{(n)} - \hat{A}h_w^{(n)}, \quad (37)$$

where the signal “+” denotes the reflected particles from the surface, while the signal “-” denotes the incident particles on the surface. For the problem in question, the source terms are given as

$$h_w^{(u)} = -2c_z, \quad h_w^{(a)} = \left(c^2 - \frac{3}{2}\right) \frac{z_0}{\delta} \cos \theta, \quad (38)$$

where $c_z = c_r \cos \theta - c_\theta \sin \theta$.

In spherical coordinates, the scattering operator \hat{A} is decomposed as

$$\hat{A}h^{(n)} = \hat{A}_r \hat{A}_\theta \hat{A}_\phi h^{(n)}, \quad (39)$$

where

$$\hat{A}_r \xi = -\frac{1}{c_r} \int_{c'_r < 0} c'_r \exp(c_r^2 - c'^2_r) R_r(c_r \rightarrow c'_r) \xi(c'_r) dc'_r, \quad (40)$$

$$\hat{A}_i \xi = \int_{-\infty}^{\infty} \exp(c_i^2 - c'^2_i) R_i(c_i \rightarrow c'_i) \xi(c'_i) dc'_i, \quad i = \theta, \phi, \quad (41)$$

for an arbitrary ξ as function of the molecular velocity. According to the scattering kernel proposed by Cercignani and Lampis [37], the functions R_r , R_θ and R_ϕ are given by

$$R_r(c_r \rightarrow c'_r) = \frac{2c_r}{\alpha_n} \exp\left[-\frac{c_r^2 + (1 - \alpha_n)c'^2_r}{\alpha_n}\right] I_0\left(\frac{2\sqrt{1 - \alpha_n}}{\alpha_n} c_r c'_r\right), \quad (42)$$

$$R_i(c_i \rightarrow c'_i) = \frac{1}{\sqrt{\pi\alpha_t(2 - \alpha_t)}} \exp\left\{-\frac{[c_i - (1 - \alpha_t)c'_i]^2}{\alpha_t(2 - \alpha_t)}\right\}, \quad i = \theta, \phi, \quad (43)$$

where I_0 denotes the modified Bessel function of first kind and zeroth order. In this model of gas-surface interaction, the accommodation coefficients can vary in the ranges $0 \leq \alpha_t \leq 2$ and $0 \leq \alpha_n \leq 1$. The case $\alpha_t=1$ and $\alpha_n=1$ corresponds to diffuse scattering or complete accommodation on the spherical

surface, while the case $\alpha_t=0$ and $\alpha_n=0$ corresponds to specular reflection at the surface.

After some algebraic manipulation, it can be shown that

$$\hat{A}_i c_i = (1 - \alpha_t) c_i, \quad i = \theta, \phi, \quad (44)$$

$$\hat{A}_i c_i^2 = (1 - \alpha_t)^2 c_i^2 + \frac{1}{2} \alpha_t (2 - \alpha_t), \quad (45)$$

$$\hat{A}_r c_r = -\sqrt{\alpha_n} H_1(\eta), \quad (46)$$

$$\hat{A}_r c_r^2 = \alpha_n + (1 - \alpha_n) c_r^2, \quad (47)$$

where

$$H_1(\eta) = 2e^{-\eta^2} \int_0^\infty \xi^2 e^{-\xi^2} I_0(2\eta\xi) d\xi, \quad \xi = \frac{c'_r}{\sqrt{\alpha_n}}, \quad (48)$$

and

$$\eta = c_r \sqrt{\frac{1}{\alpha_n} - 1}. \quad (49)$$

Therefore, from (37), the boundary conditions at $r=r_0$ for the perturbation functions of reflected gas particles, i.e. $c_r > 0$, from the spherical surface are written as

$$h^{+(u)} = \hat{A} h^{-(u)} - 2 \frac{z_0}{\delta} [(1 - \alpha_t) c_r + \sqrt{\alpha_n} H_1(\eta)] - 2 \alpha_t c_z, \quad (50)$$

$$h^{+(a)} = \hat{A} h^{-(a)} - \frac{z_0}{\delta} [\alpha_n (1 - c_r^2) + \alpha_t (2 - \alpha_t) (1 - c_t^2)]. \quad (51)$$

5. Reciprocity relation

In our previous paper [28], the reciprocal relation between the thermophoretic force and drag force solution was obtained in its explicit form. The analogous relation between the radiometric force and drag force solution is simpler and follows directly from the theory described in Ref.[48]. Then, the explicit relation was obtained in the subsequent work, see Eq.(5.42) from [49], which in our dimensionless notations reads

$$4\pi F_q = - \int_{\Sigma_w} \tau_p q_r^{(u)}(r_0, \theta) d\Sigma_w \quad (52)$$

where the temperature deviation of the particle surface τ_p is calculated from (10) and (11) as

$$\tau_p = \frac{T_p - T_0}{X_q T_0} = \cos \theta. \quad (53)$$

Considering that $d\Sigma_w = \sin \theta d\theta d\phi$ and integrating (52) with respect to ϕ , the reciprocal relation is reduced to

$$F_q = -\frac{1}{2} \int_0^\pi q_r^{(u)}(r_0, \theta) \cos \theta \sin \theta d\theta. \quad (54)$$

According to Eq.(6.16) from [28], $q_r^{(u)}$ can be represented as

$$q_r^{(u)}(r, \theta) = q_r^{*(u)}(r) \cos \theta. \quad (55)$$

Substituting (55) into (54), we obtain the reciprocal relation in its simple form

$$F_q = -\frac{1}{3} q_r^{*(u)}(r_0). \quad (56)$$

6. Force in the free molecular and continuum regimes

In the free molecular regime, i.e. $\delta \ll 1$, the perturbation function of incident gas particles on the surface is not perturbed, which means that $h^{-(n)} = h_\infty^{(n)}$ for the corresponding thermodynamic force. Thus, from (35) and (36), $h^{-(n)} = 0$ for both thermodynamic forces. Therefore, the substitution of the solution (51) into (34) leads to the following expression for the radiometric force on the sphere in the free molecular regime

$$F_q = -\frac{\alpha_n}{12}, \quad (57)$$

which depends only on the NEAC.

In the continuum regime, i.e. $\delta \gg 1$, the radiometric force is obtained from the Navier-Stokes equations with thermal slip boundary condition. Thus, according to Ref. [49], the radiometric force on the sphere reads

$$F_q = -\frac{\sigma_T}{2\delta^2}, \quad (58)$$

where σ_T is the thermal slip coefficient, which depends on the NEAC and TMAC as well as on the intermolecular interaction potential. Reliable values for the thermal slip coefficient can be found in Ref.[50].

The forces (57) and (58) satisfy the reciprocity relation (56). In the free molecular regime, the radial component of the heat flux at the boundary is obtained just by substituting (50) into (30). After some algebraic manipulation the following expression is obtained

$$q_r^{(u)}(r_0) = \frac{\alpha_n}{4}. \quad (59)$$

In the continuum regime, the heat flux cannot be obtained by the classical Navier-Stokes-Fourier equations because it appears in an approximation of second order in the Knudsen number, see e.g. [47, 51]. Thus, the reciprocity relation (56) is verified numerically by comparing the present results obtained for the radiometric force with those obtained previously [28] for the heat flux.

7. Numerical solution

Like in our previous paper [28], in order to eliminate the dependence of the numerical solution on the variables θ and ϕ' , the similarity solution proposed in Ref. [52] is employed. Thus, the dependence of the numerical scheme on the variables θ and ϕ' is eliminated by representing the perturbation function $h^{(q)}$ as

$$h^{(q)}(r, \theta, \mathbf{c}) = h_c^{(q)}(r, c, \theta') \cos \theta + h_s^{(q)}(r, c, \theta') c_\theta \sin \theta. \quad (60)$$

The substitution of this representation into the kinetic equation (23) for the thermodynamic force X_q leads to the following system of equations for the functions $h_c^{(q)}$ and $h_s^{(q)}$

$$\begin{aligned} c_r \frac{\partial h_c^{(q)}}{\partial r} - \frac{c_t}{r} \frac{\partial h_c^{(q)}}{\partial \theta'} + \frac{c_t^2}{r} h_s^{(q)} &= \nu^{*(q)} + \left(c^2 - \frac{3}{2} \right) \tau^{*(q)} + 2c_r u_r^{*(q)} \\ &+ \frac{4}{15} c_r \left(c^2 - \frac{5}{2} \right) q_r^{*(q)} - h_c^{(q)}, \end{aligned} \quad (61)$$

$$\begin{aligned} c_r \frac{\partial h_s^{(q)}}{\partial r} - \frac{c_t}{r} \frac{\partial h_s^{(q)}}{\partial \theta'} - \frac{c_r}{r} h_s^{(q)} - \frac{1}{r} h_c^{(q)} &= 2u_\theta^{*(q)} \\ &+ \frac{4}{15} \left(c^2 - \frac{5}{2} \right) q_\theta^{*(q)} - h_s^{(q)}, \end{aligned} \quad (62)$$

where the quantities with * are calculated from (26)-(31) as

$$\nu^{*(q)}(r) = \frac{\nu^{(q)}(r, \theta)}{\cos \theta} = \frac{2}{\sqrt{\pi}} \int_0^\infty \int_0^\pi c_t h_c^{(q)} e^{-c^2} c d c d \theta', \quad (63)$$

$$\tau^{*(q)}(r) = \frac{\tau^{(q)}(r, \theta)}{\cos \theta} = \frac{4}{3\sqrt{\pi}} \int_0^\infty \int_0^\pi \left(c^2 - \frac{3}{2} \right) c_t h_c^{(q)} e^{-c^2} c d c d \theta', \quad (64)$$

$$u_r^{*(q)}(r) = \frac{u_r^{(q)}(r, \theta)}{\cos \theta} = \frac{2}{\sqrt{\pi}} \int_0^\infty \int_0^\pi c_r c_t h_c^{(q)} e^{-c^2} c d c d \theta', \quad (65)$$

$$u_\theta^{*(q)}(r) = \frac{u_\theta^{(q)}(r, \theta)}{\sin \theta} = \frac{1}{\sqrt{\pi}} \int_0^\infty \int_0^\pi c_t^3 h_s^{(q)} e^{-c^2} c d c d \theta', \quad (66)$$

$$q_r^{*(q)}(r) = \frac{q_r^{(q)}(r, \theta)}{\cos \theta} = \frac{2}{\sqrt{\pi}} \int_0^\infty \int_0^\pi c_r c_t \left(c^2 - \frac{5}{2} \right) h_c^{(q)} e^{-c^2} c d c d \theta', \quad (67)$$

$$q_\theta^{*(q)}(r) = \frac{q_\theta^{(q)}(r, \theta)}{\sin \theta} = \frac{1}{\sqrt{\pi}} \int_0^\infty \int_0^\pi c_t^3 \left(c^2 - \frac{5}{2} \right) h_s^{(q)} e^{-c^2} c d c d \theta'. \quad (68)$$

The representation (60) is compatible with the CL-model of the gas-surface interaction so that

$$\hat{A} h^{-(q)} = \cos \theta \hat{A}_r \hat{A}_t^{(0)} h_c^{-(q)} + \sin \theta \cos \phi' \hat{A}_r \hat{A}_t^{(1)} h_s^{-(q)}, \quad (69)$$

where

$$\begin{aligned} \hat{A}_r \xi &= \frac{2}{\alpha_n} \int_0^\infty c'_r \exp \left[-\frac{(1 - \alpha_n) c_r^2 + c_r'^2}{\alpha_n} \right] \\ &\quad \times I_0 \left(\frac{2\sqrt{1 - \alpha_n} c_r c'_r}{\alpha_n} \right) \xi(-c'_r, c'_r) d c'_r, \end{aligned} \quad (70)$$

$$\begin{aligned} \hat{A}_t^{(i)} \xi &= \frac{2}{\alpha_t(2 - \alpha_t)} \int_0^\infty c_t'^{(i+1)} \exp \left[-\frac{(1 - \alpha_t)^2 c_t^2 + c_t'^2}{\alpha_t(2 - \alpha_t)} \right] \\ &\quad \times I_i \left[\frac{2(1 - \alpha_t) c_t c_t'}{\alpha_t(2 - \alpha_t)} \right] \xi(c'_r, c'_t) d c'_t. \end{aligned} \quad (71)$$

I_i ($i=0, 1$) is the modified Bessel function of first kind and i -th order.

Therefore, the substitution of the representation (60) into the corresponding boundary condition (51) for the thermodynamic force X_q leads to the following boundary conditions

$$h_c^{+(q)} = \hat{A}_r \hat{A}_t^{(0)} h_c^{-(q)} + \alpha_n (c_r^2 - 1) + \alpha_t (2 - \alpha_t) (c_t^2 - 1), \quad (72)$$

$$h_s^{+(q)} = \frac{1}{c_t} \hat{A}_r \hat{A}_t^{(1)} h_s^{-(q)}. \quad (73)$$

Far from the sphere, the representation (60) leads to the following asymptotic behaviors

$$\lim_{r \rightarrow \infty} h_c^{(q)} = 0, \quad (74)$$

$$\lim_{r \rightarrow \infty} h_s^{(q)} = 0. \quad (75)$$

After some algebraic manipulation, the dimensionless radiometric force on the sphere given in (34) is rewritten as

$$F_q = -\frac{1}{3} \left[\Pi_{rr}^{*(q)}(r_0) - 2\Pi_{r\theta}^{*(q)}(r_0) \right], \quad (76)$$

where

$$\Pi_{rr}^{*(q)}(r_0) = \frac{4}{\sqrt{\pi}} \int_{-\infty}^{\infty} \int_{-\infty}^{\infty} c_r^2 c_t h_c^{(q)}(r_0, c_r, c_t) e^{-c^2} dc_r dc_t, \quad (77)$$

$$\Pi_{r\theta}^{*(q)}(r_0) = \frac{2}{\sqrt{\pi}} \int_{-\infty}^{\infty} \int_{-\infty}^{\infty} c_r c_t^3 h_s^{(q)}(r_0, c_r, c_t) e^{-c^2} dc_r dc_t, \quad (78)$$

with $\Pi_{rr}^{*(q)}(r_0) \cos \theta$ and $\Pi_{r\theta}^{*(q)}(r_0) \sin \theta$ denoting the dimensionless normal and tangential stress on the sphere.

The system of kinetic equations (61)-(62) subject to the boundary conditions (72)-(73) and asymptotic behaviors (74)-(75) was solved numerically via the discrete velocity method with an accuracy of 0.1% for the moments of the perturbation functions at the boundary. Details regarding the discrete velocity method can be found in the literature, see e.g. the book by Sharipov [11]. The Gaussian quadrature was used to discretize the molecular velocity and calculate the moments of the perturbation function. The numerical values of the nodes and weights as well as the technique to calculate them are described in Ref. [53]. Moreover, a finite difference scheme was used to approximate the derivatives which appear in the kinetic equation. The accuracy was estimated by varying the grid parameters N_r , N_c and N_θ corresponding to the number of nodes in the radial coordinate r , molecular speed c and angle θ' , as well as the maximum value of the radial coordinate, denoted here as r_{max} , which defines the gas flow domain. For $\alpha_n=0.8, 0.9$ and 1, the values of these parameters were N_c and N_θ fixed at 20 and 1400, respectively, while N_r varied according to the distance r_{max} so that the increment $\Delta r \sim 10^{-3}$. For $\alpha_n=0.1$ and 0.5 the grid parameters were refined so that N_c and N_θ were fixed at 25 and 1800, respectively, while N_r varied so that the increment $\Delta r \sim 10^{-4}$. The maximum radial coordinate r_{max}

varied from 10 to 100 when the rarefaction parameter varied from 0.01 to 10. The reciprocal relation (56) was verified within the relative numerical error of 0.1% for all the values of rarefaction parameter and accommodation coefficients considered in the calculations.

8. Results and discussion

8.1. Radiometric force

Firstly, the results obtained in the present work were compared to those given in Ref. [32] for diffuse scattering, i.e. $\alpha_t=1$ and $\alpha_n=1$. Figure 2 shows the comparison, in which the dimensionless force $-F_q$ is plotted as function of the rarefaction parameter δ . In Ref. [32], the full Boltzmann equation was solved numerically via a finite-difference scheme method and the similarity solution proposed in Ref. [52]. In the present work a similar approach was employed for solving the kinetic model to the Boltzmann equation. As one can see from Figure 2, the results are in a good agreement over the whole range of rarefaction parameter considered. The advantage of using the model kinetic equation instead of the full Boltzmann equation concerns the computational effort. As it is known, in spite of the great computational infrastructure currently available, to solve the Boltzmann equation is still a difficult task so that the use of kinetic models plays an important role in the solution of problems involving rarefied gas flows. According to Figure 2, as the rarefaction parameter increases the magnitude of the radiometric force F_q decreases. Note that the force is always negative, which means a force in the z -direction, from the hotter to the colder side of the sphere.

In the free molecular regime the effects from intermolecular collisions are negligible and, consequently, the Knudsen mechanism is the only responsible for the appearance of the radiometric force on the sphere in the same direction of the gas stream velocity \mathbf{U}_∞ . Since the radiometric force is due to the momentum transfer from gas molecules to the surface, the magnitude of the force is larger in the free molecular regime where there is no momentum transfer due to molecular collisions. In fact, the larger the gas rarefaction the stronger the influence of intermolecular collisions on the net momentum transfer from gas molecules to the surface and the smaller the radiometric force on the sphere. This behavior is also valid for other values of accommodation coefficients. The analytic expression for the force on the sphere in the free molecular regime is given in (57).

As the rarefaction parameter increases, the intermolecular collisions lead to the so called thermal creep phenomenon, which means a gas flow in the thin layer around the sphere, from the colder to the hotter side of the sphere,

and induces a force on the sphere in the direction of the gas stream velocity \mathbf{U}_∞ . In the framework of the continuum equations of fluid mechanics, since the thermal creep appears only in an approximation of first order in the Knudsen number, the radiometric force is predicted only with the use of the thermal slip boundary condition and its expression is given in (58). Note that the force tends to zero when $\delta \rightarrow \infty$, which means that the thermal creep flow vanishes in this limit of rarefaction parameter. Table 1 presents the radiometric force on the sphere obtained from the solution of the kinetic equation as function of the rarefaction parameter and accommodation coefficients. The range of gas rarefaction considered in the calculations covers the free molecular, transition and continuum regimes. The limit solutions obtained analytically in the free molecular and continuum regimes are also presented in Table 1 for comparison. Since the force given in (58) depends on the thermal slip coefficient, the data available in Ref. [50] were used. Nonetheless, the thermal slip coefficient is sensitive to both accommodation coefficients and it was not possible to find the values of this coefficient for all the sets of accommodation coefficients considered in Table 1. According to Table 1, for diffuse scattering and $\delta=10$, the relative difference between the results obtained from the numerical solution of the kinetic equation and that obtained from the analytic expression (58) is less than 10%. Thus, for $\delta > 10$, the expression (58) can be used because this relative difference is within 10% when diffuse scattering is assumed. However, it is important to point out that in the vicinity of the boundary other non-equilibrium phenomena of second order in the Knudsen number arise and influence the magnitude of the radiometric force, e.g. the so called thermal stress slip flow firstly introduced by Sone [8]. For particles with high thermal conductivity related to that of the gas, this effect is dominant and, as pointed out in our previous work [28], it can explain the appearance of the negative thermophoresis in the continuum regime.

In order to analyse the influence of the NEAC and TMAC on the radiometric force, some numerical results are presented in Table 1 for $\alpha_n=0.1, 0.5, 0.8, 0.9$ and 1, and $\alpha_t=0.5, 0.8, 0.9$ and 1. These values of accommodation coefficients were chosen because, in practice, the coefficients vary in the ranges $0.1 \leq \alpha_n \leq 1$ and $0.6 \leq \alpha_t \leq 1$ for some gases, see e.g. Ref. [39].

It is worth noting that, for all the values of rarefaction parameter considered in the tabulated results, the reciprocity relation (56) is fulfilled for all the sets of accommodation coefficients. The relative difference between the radiometric force given in Table 1 and those values obtained from Table 3 is within 0.1%.

According to Table 1, the influence of the TMAC on the force when $\delta=0.01$ is negligible and the results tend to those predicted by the expression

(57) in the free molecular limit. In case of $\delta=0.1$ one can also say that the influence of the TMAC is negligible because the maximum deviation from the corresponding value of the force in case of diffuse scattering is less than 0.1% when α_t varies from 1 to 0.5, but it is around 90% when α_n varies from 1 to 0.1. As the rarefaction parameter increases, the influence of the TMAC on the force increases, while the influence of the NEAC decreases. For instance, for $\delta=1$, the results presented in Table 1 show that the maximum difference from diffuse scattering is around 3% when α_t varies from 1 to 0.5, and 85% when α_n varies from 1 to 0.1. For $\delta=10$, the maximum difference from diffuse scattering is around 22% when α_t varies from 1 to 0.5, and 79% when α_n varies from 1 to 0.1. The comparison with the results obtained from (58) shows that the relative difference between the numeric and analytic results for $\delta=10$ is larger than 10% for the sets of accommodation coefficients considered. As pointed out previously, this difference can be explained by the existence of other non-equilibrium phenomena of second order in the Knudsen number whose contribution were not considered in the analytic procedure to obtain (58).

Regarding the qualitative behavior of the force on the accommodation coefficients, the results show us that for fixed values of the TMAC the force increases by increasing the NEAC at arbitrary values of the gas rarefaction. Nonetheless, for fixed values of the NEAC, Table 1 shows that the force decreases by increasing the TMAC when $\delta=1$ and 10 in the range $0.5 \leq \alpha_n \leq 1$, while the opposite behavior occurs when $\alpha_n=0.1$. Moreover, note that in case of $\delta=0.1$, although the influence of the TMAC on the force is negligible, the force always increases by increasing the TMAC. This behavior can be better explained by visualizing the profiles of the normal and tangential stress on the sphere as functions of the TMAC and fixed values of the NEAC. According to (76), the force on the sphere has the contribution of the normal and tangential stress on the spherical surface, which are given by the dimensionless quantities $\Pi_{rr}^{*(q)}(r_0)$ and $\Pi_{r\theta}^{*(q)}(r_0)$. Figure 3 shows the profiles of $\Pi_{rr}^{*(q)}(r_0)$ and $\Pi_{r\theta}^{*(q)}(r_0)$ as functions of the TMAC for $\delta=0.1$, 1 and 10, respectively, by considering fixed values of the NEAC, namely $\alpha_n=0.1, 0.3, 0.5, 0.8$ and 1. As one can see from Figure 3, an increase of the TMAC leads to a small increase of the normal stress $\Pi_{rr}^{*(q)}$ on the sphere when $\delta=0.1$ and 1 for all the values of the NEAC, while a decrease occurs when $\delta=10$. On the other hand, an increase of the TMAC can lead either to an increase or a decrease of the tangential stress on the sphere as the rarefaction parameter and the NEAC vary. For instance, when $\delta=1$ and $\alpha_n=0.1$, the tangential stress on the sphere achieves a maximum and then decreases as the TMAC varies from 0.1 to 1. Moreover, note that in this case, the tangential stress on the sphere is

negative. Thus, the behavior of both the normal and tangential stress on the sphere as the NEAC and TMAC vary explain the qualitative behavior of the force given in Table 1 when $\delta=1$ and $\alpha_n=0.1$. A similar analysis can be done for other values of rarefaction parameter and accommodation coefficients.

8.2. Flow fields

The flow fields, i.e. the macroscopic characteristics of the gas flow around the sphere corresponding to bulk velocity and heat flux in the z -direction, density and temperature deviations from equilibrium, are quantities which depend on the accommodation coefficients. To analyse the dependence of the flow fields on the accommodation coefficients, the profiles of the radial and polar components of the bulk velocity and heat flux as well as the density and temperature deviations from equilibrium, as functions of the distance r/δ are given in Figures 4-11 for $\delta=0.001, 0.1, 1$ and 10 . Note that, according to the definitions given in (5) and (13), the dimensionless distance r/δ corresponds to the ratio of the dimensional radial coordinate r' to the radius of the sphere R_0 . The dependence on the TMAC is showed in Figures 4, 6, 8 and 10, with the NEAC fixed at $\alpha_n=1$. The dependence on the NEAC is showed in Figures 5, 7, 9 and 11, with the TMAC fixed at $\alpha_t=1$. As one can see from these figures, the dependence of the flow fields on the NEAC is stronger than that corresponding to the TMAC. In some situations even the qualitative behavior of the gas flow is different from that corresponding to diffuse scattering, see e.g. the radial and polar components of the bulk velocity given in Figures 5, 7 and 9 for $\delta=0.001, 0.1$ and 1 , respectively, and $\alpha_t=1$. According to Figures 5, 7 and 9, in case of diffuse scattering, the temperature distribution on the sphere leads to a gas flow towards the positive z -direction when $\delta=0.1$ and 1 , and the the absence of motion when $\delta=0.001$. However, the qualitative behavior of the gas flow can be totally different when $\alpha_n \neq 1$. For instance, from Figure 5, one can see that, actually, there is gas motion around the sphere in the free molecular regime when $\alpha_t=1$ and $\alpha_n \neq 1$. Moreover, such a flow is towards the negative z -direction. From Figure 7, corresponding to $\delta=0.1$, one can also see that the gas flow is in the negative z -direction when $\alpha_n=0.1$. Nonetheless, when $\alpha_n=0.5$ and 0.8 the gas flow changes direction in the layer adjacent to the sphere so that a clockwise vortex appears. For $\delta=1$, Figure 9 shows a similar behavior when $\alpha_n=0.1$. For a better visualization, the speed contour and velocity streamlines are given in Figures 12-14 for $\delta=0.1, 1$ and 10 , $\alpha_t=1$, $\alpha_n=0.1$ and 0.5 . These figures clearly show that the flow pattern around the sphere can drastically change as the NEAC varies in the free molecular and transition regime. For fixed values of the NEAC a change in the flow pattern is also observed when the rarefaction parameter changes. For instance, when $\delta=10$ the gas flows towards the positive z -

direction when $\alpha_n=0.1$. However, a clockwise vortex appears in the vicinity of the boundary when $\delta=1$, and the transition of the flow pattern from the positive to the negative z -direction is complete when $\delta=0.1$. This kind of change in the flow pattern as the accommodation coefficients vary in the free molecular and transition regimes was already observed in Ref. [36] for a planar geometry.

From Figures 4, 6, 8 and 10 one can see that the temperature and density deviations from equilibrium did not depend on the TMAC in the whole range of the gas rarefaction. According to these figures, while the temperature deviation increases near the sphere, the density deviation decreases. On the other hand, Figures 5, 7, 9 and 11 show a dependence of these quantities on the NEAC. For $\delta=10$ the temperature deviation increases while the density deviation decreases near the sphere. However, for other values of the gas rarefaction, only the qualitative behavior of the temperature deviation is the same. As one can see, when $\delta=0.001, 0.1$ and 1 , the density deviation decreases near the sphere when $\alpha_n \geq 0.5$, but when $\alpha_n=0.1$ there is an increase of the density deviation in the thin layer adjacent to the sphere.

8.3. Comparison with experiment

In practice, the thermal polarization on the spherical particle is measured, i.e. the temperature drop between the ends of the sphere diameter parallel to the gas stream velocity \mathbf{U}_∞ . Here, this temperature drop is obtained from (10) as

$$\Delta T' = 2T_0\tau_{s0}, \quad (79)$$

where $\tau_{s0}=X_q$.

The condition (8) allows us to relate the thermodynamic forces X_q and X_u so that

$$X_q = -q_r^{*(u)}(r_0) \left[q_r^{*(q)}(r_0) + \frac{15\Lambda}{8\delta} \right]^{-1} X_u, \quad (80)$$

where the values for the radial components of the heat flux at the surface, $q_r^{*(q)}(r_0)$ and $q_r^{*(u)}(r_0)$, due to each thermodynamic force are given in Tables 2 and 3 for some values of rarefaction parameter and accommodation coefficients. Note that, in the free molecular regime, while $q_r^{*(u)}(r_0)$ does not depend on the TMAC, $q_r^{*(q)}(r_0)$ depends on both accommodation coefficients. Moreover, in the limit $\Lambda \rightarrow \infty$ corresponding to a sphere with high thermal conductivity related to that of the carrier gas, $\Delta T \rightarrow 0$ for arbitrary values of rarefaction parameter so that the thermal polarization of the spherical particle can be neglected.

For convenience, from (79) and (80), the following dimensionless temperature drop is introduced as

$$\Delta T = \frac{\Delta T'}{T_0 X_u} = -2q_r^{*(u)}(r_0) \left(q_r^{*(g)}(r_0) + \frac{15 \Lambda}{8 \delta} \right)^{-1}. \quad (81)$$

Figures 15 and 16 show the results for the temperature drop ΔT as function of the rarefaction parameter δ , in the range $0 < \delta \leq 10$, for a Pyrex glass sphere in helium ($\Lambda=7.5$) and argon ($\Lambda=62.5$) gas. The experimental data provided in Ref. [6] are presented in these figures for comparison. It is worth noting that these experimental data did not cover the whole range of the gas rarefaction we are interested in. While for helium the data cover the range $3 < \delta \leq 10$, for argon the range is reduced to $6 < \delta \leq 10$. The experimental apparatus employed in Ref. [6] consisted of a 6 mm radius sphere suspended by a differential thermocouple in the center of a tube 1.8 m long and 0.12 m in diameter mounted in a thermostatically controlled box. The pressure of the system was adjusted to vary in the range from 1 to 100 Pa, while a gas handling system allowed to provide a volume flow within the range from 0 to 20 cm³/s corresponding to Mach number from 10^{-2} to 10^{-3} . The thermocouple signal was recorded by a set of instruments so that the value of the temperature drop between the ends of the sphere was measured at different values of Mach number and various values of fixed gas pressures in the tube. The dimensionless temperature drop introduced in Ref. [6], which is denoted by ΔT^* , as function of the Knudsen number, $Kn = \sqrt{\pi}/(2\delta)$, is related to the temperature drop defined in (81) as

$$\Delta T = \frac{\pi}{2\delta} \frac{\Delta T^*}{(\Lambda + 2)}. \quad (82)$$

According to the literature, see e.g. Ref. [50], the TMAC of helium and argon at a glass surface supported by experiments is close to 0.9, while no values were found for the NEAC of both gases at the same surface. However, it is known that the NEAC of helium in clean metallic surfaces is close to 0.1, while in case of argon is close to 0.6. Thus, the temperature drop was calculated for diffuse scattering and for other sets of accommodation coefficients with the TMAC fixed at 0.9 and the NEAC varying in the range $0.1 \leq \alpha_n \leq 1$. Figures 15 and 16 show the temperature drop ΔT as function of the rarefaction parameter for some sets of accommodation coefficients.

According to Figure 15, corresponding to helium, the numerical results are in good agreement with the experimental data provided by Ref. [6] when $\alpha_t=0.9$ and $\alpha_n=0.4$. However, the experimental data did not cover all the range of the gas rarefaction considered in the numerical calculations. For

argon, as one can see from Figure 16, a good agreement with experimental data is observed when $\alpha_t=0.9$ and $\alpha_n=0.8$ and just one experimental point is closer to the theoretical results corresponding to $\alpha_n=0.6$. Nonetheless, it is worth noting that the range of rarefaction parameter covered by the experiment with argon gas is smaller than that corresponding to helium gas. As expected, since the thermal conductivity of argon is smaller than that corresponding to helium, the thermal polarization effect of the spherical particle is stronger in helium. Moreover, note that the temperature drop has a non-linear behavior in the rarefaction parameter. According to Figures 15 and 16, the thermal polarization of the Pyrex glass sphere in both gases is stronger when the rarefaction parameter is in the range $2 < \delta < 4$.

9. Concluding remarks

In the present work, the radiometric force acting on a spherical particle with arbitrary thermal conductivity, as well as the flow fields around it, were calculated on the basis of the linearized kinetic equation proposed by Shakhov and the Cercignani-Lampis model of gas-surface interaction. The kinetic equation was solved by using the discrete velocity method in a range of the gas rarefaction covering the free molecular, transition and continuum regimes, and for some sets of accommodation coefficients. The reciprocity relation between the cross phenomena was obtained and verified numerically within the numerical error. The results show a significant dependence of the force and flow fields on the TMAC and NEAC. For fixed values of the TMAC, the force always increases by increasing the NEAC. However, for fixed values of the NEAC, the qualitative behavior of the force depends on the values of the TMAC and rarefaction parameter. In the free molecular regime the radiometric force is independent of the TMAC, while in the transition and continuum regimes this force strongly depends on both accommodation coefficients, and it can change even qualitatively its behavior. The gas flow pattern around the sphere is also strongly dependent on the accommodation coefficients. The absence of gas motion around the sphere under the diffuse scattering predicted previously is observed. However, for non-diffuse scattering there is indeed a gas flow around the sphere. The dominant gas flow can be directed in the positive z -direction with the counterclockwise vortex in the vicinity of the sphere. In some situations, the flow direction is opposite, i.e. the vortex is clockwise.

The results for the temperature drop between the two diametrically opposite points on the spherical surface in the z -direction was calculated and compared with experimental data for a Pyrex glass in helium and argon. The comparison shows a good agreement between the numerical and experimen-

tal results when appropriate values for the NEAC and TMAC are used. The results obtained in the present work show the importance of the gas-surface interaction law for the correct modelling of the physics underlying the movement of small particles in a rarefied gas, such as aerosols in the atmosphere and in technological applications.

Declaration of Competing Interest

The authors declare that they have no competing financial interests or personal relationships that could have appeared to influence the work reported in this paper.

Acknowledgments

D. Kalempa acknowledges FAPESP (Fundação de Amparo à Pesquisa do Estado de São Paulo) for the support of the research, grant 2015/20650-5. F. Sharipov acknowledges CNPq (Conselho Nacional de Desenvolvimento Científico e Tecnológico), grant 304831/2018-2.

References

- [1] E H Kennard. *Kinetic Theory of Gases*. McGraw-Hill Book Company, Inc., New York, 1938.
- [2] Y Sone. Thermal creep in rarefied gas. *J. Phys. Soc. Jpn*, 21:1836–1837, 1966.
- [3] B K Annis. Thermal creep in gases. *J. Chem. Phys.*, 57(7):2898–2905, 1972.
- [4] S K Loyalka. Slip in the thermal creep flow. *Phys. Fluids*, 14(11):21–24, 1971.
- [5] S P Bakanov, V V Vysotskij, B V Derjaguin, and V I Roldughin. Thermal polarization of bodies in the rarefied gas flow. *J. Non-Equilib. Thermodyn*, 8:75–84, 1983.
- [6] S P Bakanov and Vysotskij. Thermal polarization of bodies in the rarefied gas flow and thermophoresis of aerosols. *J. Aerosol Sci.*, 25 SI:407–408, 1994.
- [7] L D Landau and E M Lifshitz. *Fluid Mechanics*. Pergamon, New York, 1989.

- [8] Y Sone. Flow induced by thermal stress in rarefied gas. *Phys. Fluids*, 15:1418–1423, 1972.
- [9] R W Bosworth, A L Ventura, A D Ketsdever, and S F Gimelshein. Measurement of negative thermophoretic force. *J. Fluid Mech.*, 805:207–221, 2016.
- [10] C Cercignani. *Theory and Application of the Boltzmann Equation*. Scottish Academic Press, Edinburgh, 1975.
- [11] F Sharipov. *Rarefied Gas Dynamics. Fundamentals for Research and Practice*. Wiley-VCH, Berlin, 2016.
- [12] P L Bhatnagar, E P Gross, and M A Krook. A model for collision processes in gases. *Phys. Rev.*, 94:511–525, 1954.
- [13] E M Shakhov. Generalization of the Krook kinetic relaxation equation. *Fluid Dynamics*, 3(5):95–96, 1968.
- [14] G A Bird. *Molecular Gas Dynamics and the Direct Simulation of Gas Flows*. Oxford University Press, Oxford, 1994.
- [15] W Crookes. On attraction and repulsion resulting from radiation. *Phil. Trans. R. Soc.*, 164:501–527, 1874.
- [16] A E Woodruff. William Crookes and the Radiometer. *Isis*, 57(2):188–198, 1966.
- [17] S G Brush and C W Everitt. Maxwell, Osborne Reynolds, and the Radiometer. *Hist. Stud. Phys. Sci.*, 1:105–125, 1969.
- [18] J C Maxwell. On stresses in rarefied gases arising from inequalities of temperature. *Phil. Trans. R. Soc.*, 170:231–256, 1879.
- [19] O Reynolds. On the force caused by communication of heat between a surface and a gas, and a new photometer. *Proc. R. Soc.*, 24:387–391, 1876.
- [20] A Ketsdever, N Gimelshein, S Gimelshein, and N Selden. Radiometric phenomena: From the 19th to the 21st century. *Vacuum*, 86(11, SI):1644–1662, 2012.
- [21] Xiaowei Wang, Tianyi Su, Wenqing Zhang, Zhijun Zhang, and Shiwei Zhang. Knudsen pumps: a review. *Microsystems & Nanoengineering*, 6(1):26, June 2020.

- [22] Ahmadreza Mahyari, M. Barzegar Gerdroodbary, M. Mosavat, and D.D. Ganji. Detection of ammonia gas by Knudsen thermal force in micro gas actuator. *Case Studies in Thermal Engineering*, 12:276–284, 2018.
- [23] A. Hassanvand, M. Barzegar Gerdroodbary, Rasoul Moradi, and Younes Amini. Application of Knudsen thermal force for detection of inert gases. *Results in Physics*, 9:351–358, 2018.
- [24] Y Sone. Flows induced by temperature fields in a rarefied gas and their ghost effect on the behavior of a gas in the continuum limit. *Annu. Rev. Fluid Mech.*, 32:779–811, 2000.
- [25] M. Knudsen. *Radiometer pressure and coefficient of accommodation*, volume 11 of *Kgl. Danske Vidensk. Selskab*. A. F. Høst & søn, 1930.
- [26] Pavel Zemánek, Giorgio Volpe, Alexandr Jonáš, and Oto Brzobohatý. Perspective on light-induced transport of particles: from optical forces to phoretic motion. *Adv. Opt. Photon.*, 11(3):577–678, Sep 2019.
- [27] S A Beresnev, V G Chernyak, and G A Fomyagin. Motion of a spherical-particle in a rarefied-gas. Part 2. Drag and thermal polarization. *J. Fluid Mech.*, 219:405–421, 1990.
- [28] D Kalempa and F Sharipov. Drag and thermophoresis on a sphere in a rarefied gas based on the Cercignani-Lampis scattering model of gas-surface interaction. *J. Fluid Mech.*, 900:A37, 2020.
- [29] J C Maxwell. On stress in rarefied gases arising from inequalities of temperature. *Phil Trans. R. Soc. Lond.*, 170:231–256, 1879.
- [30] Y. Sone. Highly rarefied gas around a group of bodies with various temperature distributions. I - Small temperature variation. *Journal de Mecanique Theorique et Appliquee*, 3(2):315–328, 1984.
- [31] C Cercignani, A Frezzotti, and M N Kogan. On the absence of motion in certain nonequilibrium states of gases and vapors in free molecular regime: General considerations and pipe flow. *Phys. Fluids A*, 5(10):2551–2556, 1993.
- [32] S Takata and Y Sone. Flow induced around a sphere with a non-uniform surface temperature in a rarefied gas, with application to the drag and thermal force problem of a spherical particle with an arbitrary thermal conductivity. *Eur. J. Mech. B/Fluids*, 14(4):487–518, 1995.

- [33] F Sharipov. Application of the Cercignani-Lampis scattering kernel to calculations of rarefied gas flows. III. Poiseuille flow and thermal creep through a long tube. *Eur. J. Mech. B / Fluids*, 22:145–154, 2003.
- [34] H H Podgursky and F N Davis. Thermal transpiration at low pressure. the vapor pressure of xenon below 90 k. *J. Phys. Chem.*, 65(8):1343–1348, 1961.
- [35] T Edmonds and J P Hobson. A study of thermal transpiration using ultrahigh-vacuum techniques. *J. Vac. Sci. and Technol.*, 2(1):182–197, 1965.
- [36] S Kosuge, K Aoki, S Takata, R Hattori, and D Sakai. Steady flows of a highly rarefied gas induced by nonuniform wall temperature. *Phys. Fluids*, 23(3), 2011.
- [37] C Cercignani and M Lampis. Kinetic model for gas-surface interaction. *Transp. Theory and Stat. Phys.*, 1:101–114, 1971.
- [38] Y G Semyonov, S F Borisov, and P E Suetin. Investigation of heat transfer in rarefied gases over a wide range of Knudsen numbers. *Int. J. Heat Mass Transfer*, 27(10):1789–1799, 1984.
- [39] F Sharipov and M Moldover. Energy accommodation coefficient extracted from acoustic resonator experiments. *J. Vac. Sci. Technol. A*, 34(6):061604, 2016.
- [40] Wayne M. Trott, Jaime N. Castaneda, John R. Torczynski, Michael A. Gallis, and Daniel J. Rader. An experimental assembly for precise measurement of thermal accommodation coefficients. *Rev. Sci. Instrum.*, 82(3):035120, 2011.
- [41] O V Sazhin, S F Borisov, and F Sharipov. Accommodation coefficient of tangential momentum on atomically clean and contaminated surfaces. *J. Vac. Sci. Technol. A*, 19(5):2499–2503, 2001. Erratum: **20** (3), 957 (2002).
- [42] C Cercignani. The Kramers problem for a not completely diffusion wall. *J. Math. Anal. Appl.*, 10:568–586, 1965.
- [43] I A Graur and A Ph Polikarpov. Comparison of different kinetic models for the heat transfer problem. *Heat Mass Transf.*, 46(2):237–244, 2009.

- [44] V E Ambrus, F Sharipov, and V Sofonea. Comparison of the shakhov and ellipsoidal models for the boltzmann equation and dsmc for ab initio-based particle interactions. *Computers and Fluids*, 211:104637, 2020.
- [45] S Beresnev and V Chernyak. Thermophoresis of a spherical particle in a rarefied-gas: Numerical analysis based on the model kinetic equations. *Phys. Fluids*, 7(7):1743–1756, 1995.
- [46] E M Shakhov. Boltzmann equation and moment equations in curvilinear coordinates. *Fluid Dynamics*, 2(2):107–109, 1967.
- [47] J H Ferziger and H G Kaper. *Mathematical Theory of Transport Processes in Gases*. North-Holland Publishing Company, Amsterdam, 1972.
- [48] F Sharipov. Onsager-Casimir reciprocity relations for open gaseous systems at arbitrary rarefaction. I. General theory for single gas. *Physica A*, 203:437–456, 1994.
- [49] F Sharipov. Onsager-Casimir reciprocity relations for open gaseous systems at arbitrary rarefaction. II. Application of the theory for single gas. *Physica A*, 203:457–485, 1994.
- [50] F Sharipov. Data on the velocity slip and temperature jump on a gas-solid interface. *J. Phys. Chem. Ref. Data*, 40(2):023101, 2011.
- [51] S Chapman and T G Cowling. *The Mathematical Theory of Non-Uniform Gases*. University Press, Cambridge, 3 edition, 1970.
- [52] Y Sone and K Aoki. A similarity solution of the linearized Boltzmann equation with application to thermophoresis of a spherical particle. *Journal de Mecanique Theorique et Appliquee*, 2(1):3–12, 1983.
- [53] V I Krylov. *Approximate Calculation of Integrals*. Dover Publication Inc., Mineola, 2005.

		$-F_q$				
	α_t	$\alpha_n=0.1$	0.5	0.8	0.9	1.0
$\delta \rightarrow 0^a$	—	0.008333	0.04167	0.06667	0.07500	0.08333
$\delta=0.01$	0.5	0.008408	0.04166	0.06658	0.07489	0.08319
	0.8	0.008444	0.04169	0.06660	0.07491	0.08321
	0.9	0.008451	0.04169	0.06661	0.07491	0.08322
	1.0	0.008456	0.04170	0.06661	0.07491	0.08322
$\delta=0.1$	0.5	0.008848	0.04125	0.06547	0.07354	0.08162
	0.8	0.009114	0.04142	0.06556	0.07360	0.08164
	0.9	0.009169	0.04145	0.06557	0.07361	0.08164
	1.0	0.009206	0.04147	0.06559	0.07360	0.08164
$\delta=1$	0.5	0.008023	0.03170	0.04906	0.05475	0.06041
	0.8	0.008579	0.03140	0.04812	0.05369	0.05914
	0.9	0.008687	0.03127	0.04783	0.05336	0.05875
	1.0	0.008750	0.03114	0.04755	0.05303	0.05838
$\delta=10$	0.5	0.001076	0.004486	0.006530	0.007134	0.007705
	0.8	0.001220	0.004008	0.005694	0.006193	0.006664
	0.9	0.001278	0.003924	0.005542	0.006017	0.006464
	1.0	0.001335	0.003875	0.005429	0.005884	0.006312
$\delta=10^b$	0.5	—	0.005405	—	—	0.005860
	1.0	—	0.005875	—	—	0.005875

^a Eq. (57), free molecular regime.

^b Eq. (58), slip flow regime.

Table 1: Dimensionless radiometric force vs. rarefaction parameter and accommodation coefficients.

	α_t	$q_r^{*(q)}$				
		$\alpha_n=0.1$	0.5	0.8	0.9	1.0
$\delta \rightarrow 0^a$	0.5	0.2398	0.3526	0.4372	0.4654	0.4937
	0.8	0.2990	0.4118	0.4965	0.5247	0.5529
	0.9	0.3075	0.4203	0.5049	0.5331	0.5614
	1.0	0.3103	0.4231	0.5078	0.5360	0.5642
$\delta=0.01$	0.5	0.2397	0.3524	0.4369	0.4651	0.4932
	0.8	0.2988	0.4115	0.4961	0.5242	0.5524
	0.9	0.3073	0.4200	0.5045	0.5327	0.5608
	1.0	0.3101	0.4228	0.5073	0.5355	0.5637
$\delta=0.1$	0.5	0.2387	0.3505	0.4341	0.4620	0.4898
	0.8	0.2974	0.4089	0.4924	0.5202	0.5479
	0.9	0.3057	0.4173	0.5007	0.5285	0.5562
	1.0	0.3085	0.4200	0.5035	0.5312	0.5590
$\delta=1$	0.5	0.2287	0.3314	0.4067	0.4314	0.4560
	0.8	0.2819	0.3826	0.4564	0.4808	0.5048
	0.9	0.2894	0.3899	0.4634	0.4876	0.5116
	1.0	0.2919	0.3923	0.4658	0.4899	0.5139
$\delta=10$	0.5	0.1518	0.1952	0.2210	0.2286	0.2358
	0.8	0.1733	0.2111	0.2339	0.2406	0.2469
	0.9	0.1760	0.2131	0.2355	0.2422	0.2484
	1.0	0.1769	0.2138	0.2361	0.2427	0.2489

^a Analytic solution in the free molecular regime obtained by substituting (51) into (30).

Table 2: Dimensionless radial component of the heat flux on the spherical surface due to the force X_q .

		$q_r^{*(u)}$				
	α_t	$\alpha_n=0.1$	0.5	0.8	0.9	1.0
$\delta \rightarrow 0^a$	—	0.02500	0.1250	0.2000	0.2250	0.2500
$\delta=0.01$	0.5	0.02521	0.1250	0.1997	0.2247	0.2496
	0.8	0.02531	0.1250	0.1998	0.2247	0.2496
	0.9	0.02533	0.1250	0.1998	0.2247	0.2496
	1.0	0.02535	0.1251	0.1998	0.2247	0.2497
$\delta=0.1$	0.5	0.02653	0.1237	0.1964	0.2206	0.2449
	0.8	0.02734	0.1242	0.1966	0.2208	0.2449
	0.9	0.02751	0.1243	0.1966	0.2208	0.2449
	1.0	0.02762	0.1243	0.1966	0.2207	0.2449
$\delta=1$	0.5	0.02405	0.09506	0.1472	0.1644	0.1816
	0.8	0.02574	0.09411	0.1444	0.1610	0.1775
	0.9	0.02606	0.09375	0.1435	0.1600	0.1763
	1.0	0.02625	0.09334	0.1427	0.1590	0.1752
$\delta=10$	0.5	0.003225	0.01345	0.01961	0.02143	0.02315
	0.8	0.003656	0.01199	0.01707	0.01859	0.02001
	0.9	0.003832	0.01177	0.01661	0.01806	0.01941
	1.0	0.004007	0.01163	0.01627	0.01766	0.01894

^a Eq. (59), free molecular regime.

Table 3: Dimensionless radial component of the heat flux on the spherical surface due to the force X_u .

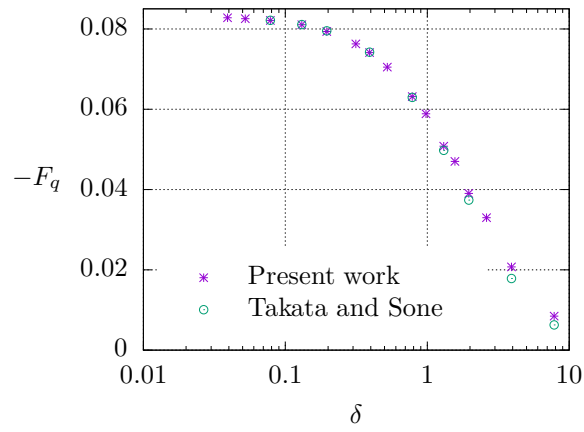


Figure 2: Radiometric force versus rarefaction parameter: comparison to the results by Takata and Sone [32], diffuse scattering.

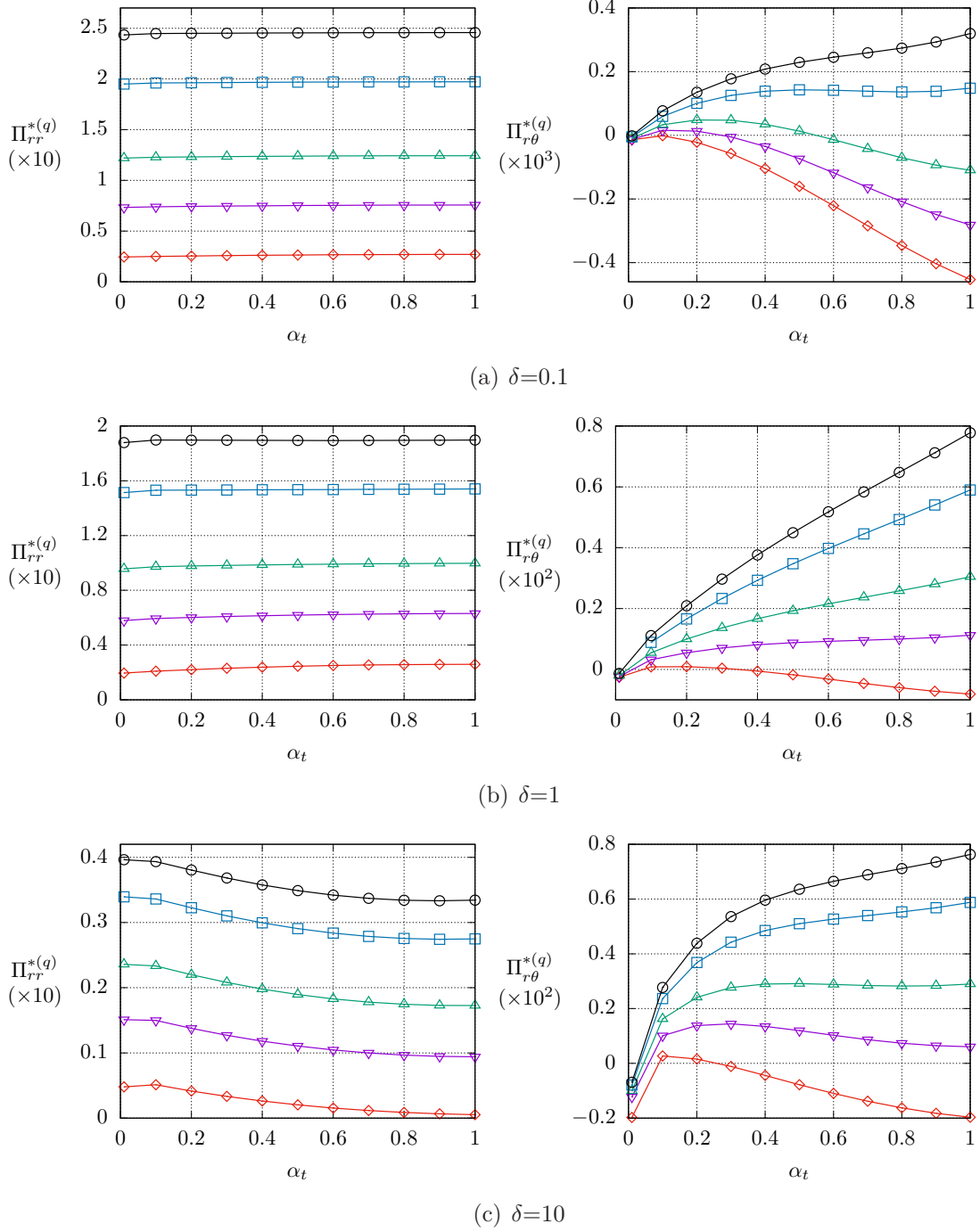
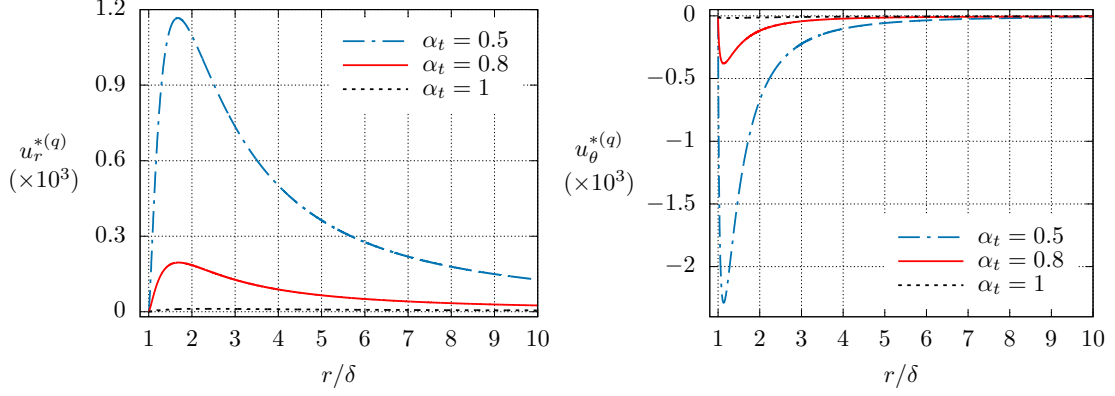
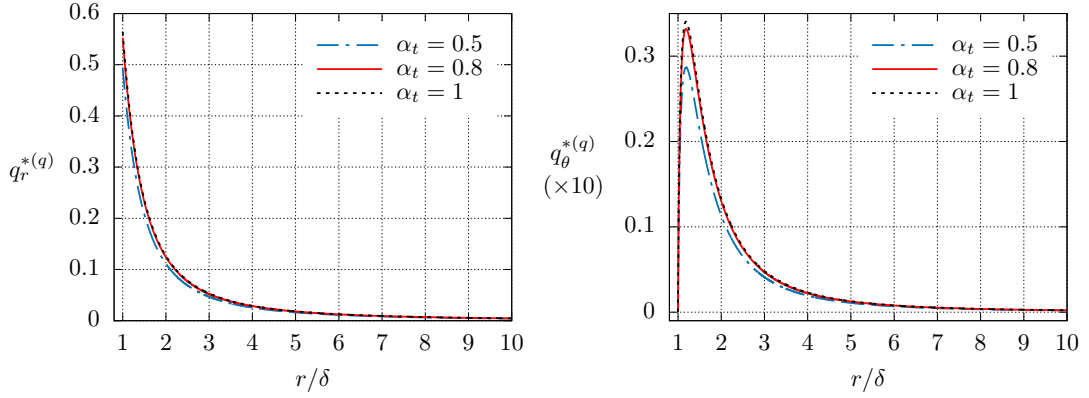


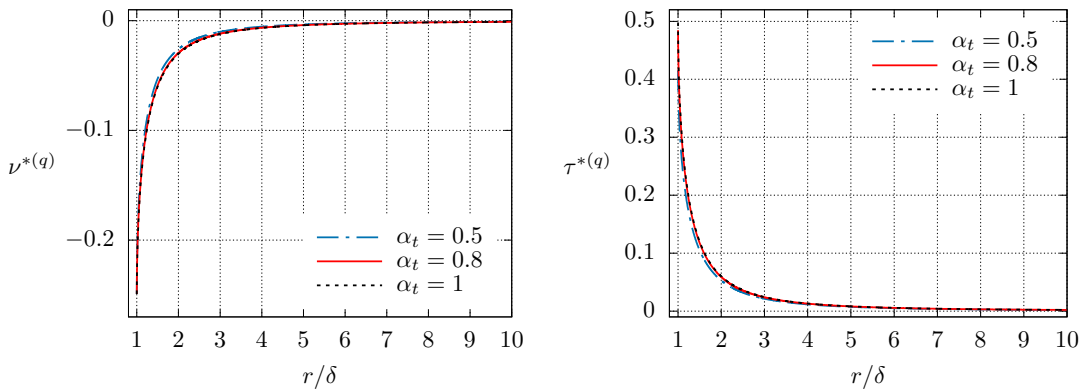
Figure 3: Normal and tangential stress on the sphere as function of the TMAC at fixed values of the NEAC. Symbols: \circ - $\alpha_n=1$; \square - $\alpha_n=0.8$; \triangle - $\alpha_n=0.5$; ∇ - $\alpha_n=0.3$; \diamond - $\alpha_n=0.1$.



(a) Radial and polar components of the bulk velocity

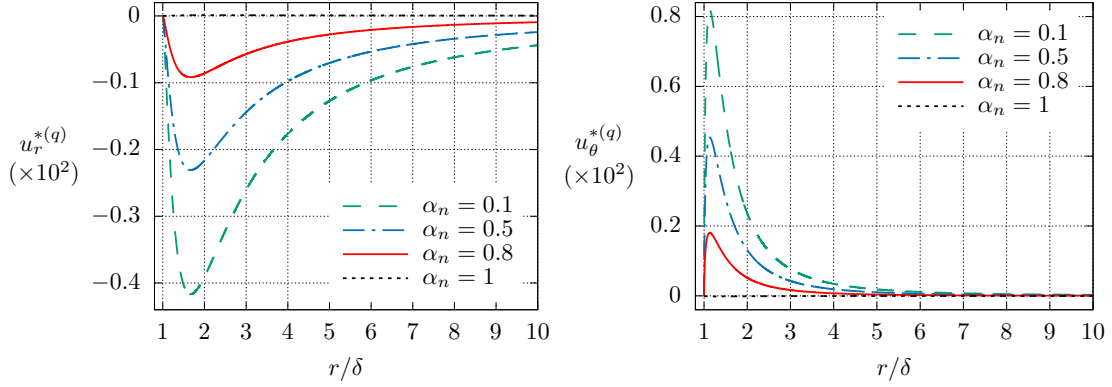


(b) Radial and polar components of the heat flux

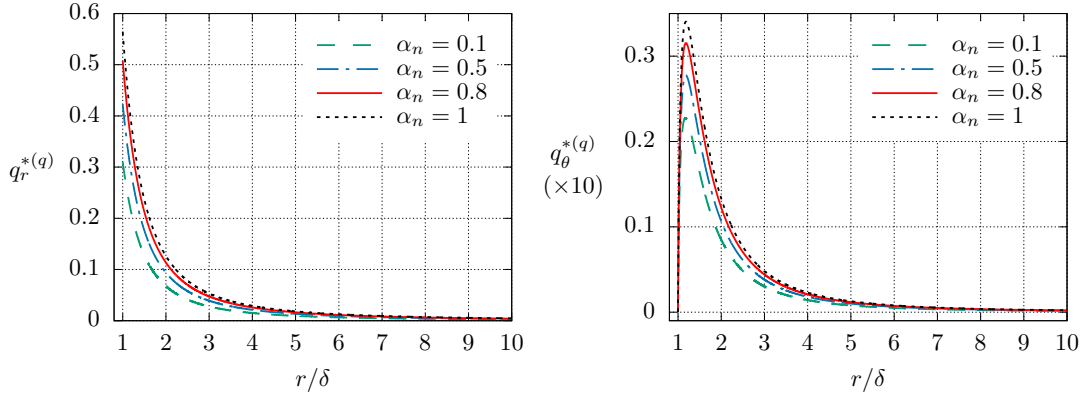


(c) Density and temperature deviations from equilibrium

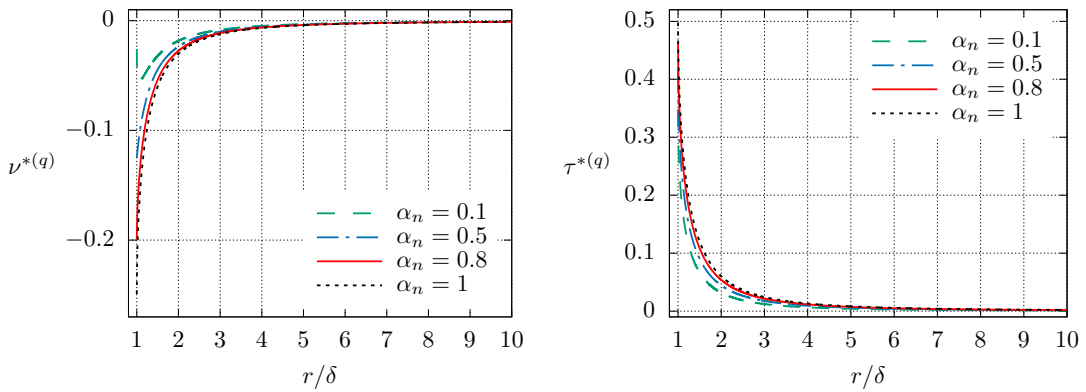
Figure 4: Flow fields due to the thermodynamic force X_q for fixed $\alpha_n=1$ and $\delta=0.001$.



(a) Radial and polar components of the bulk velocity

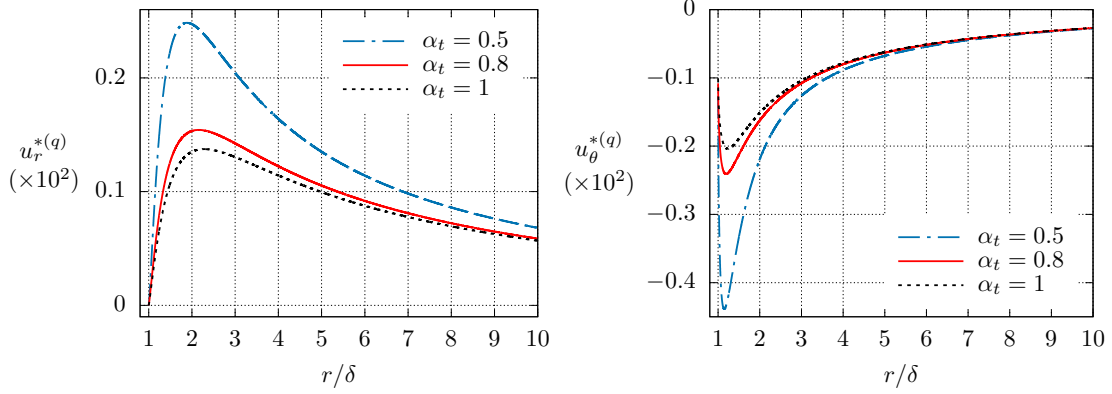


(b) Radial and polar components of the heat flux

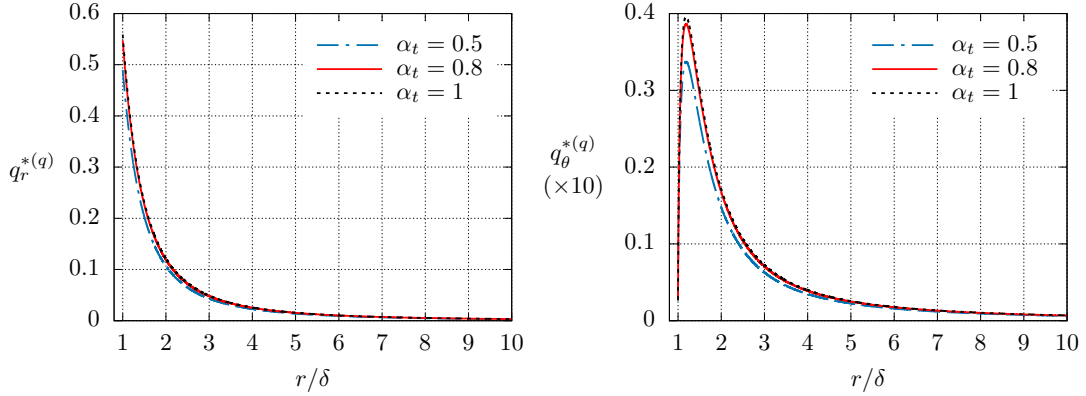


(c) Density and temperature deviations from equilibrium

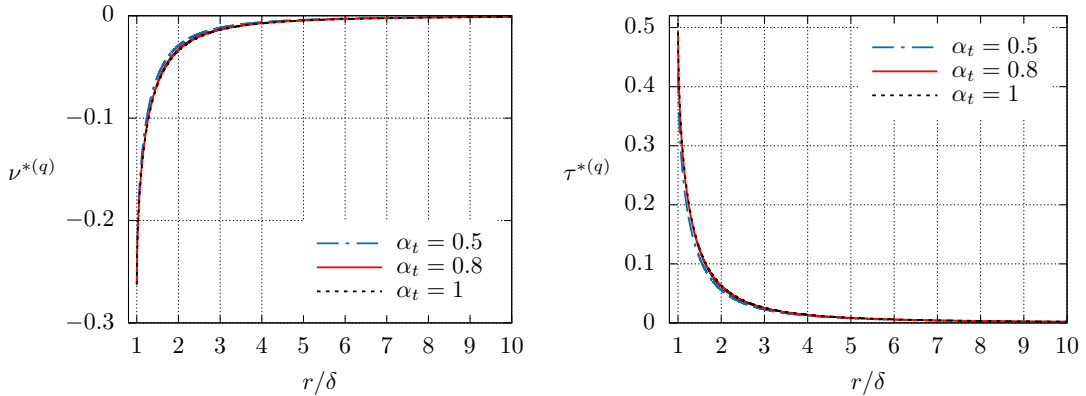
Figure 5: Flow fields due to the thermodynamic force X_q for fixed $\alpha_t=1$ and $\delta=0.001$.



(a) Radial and polar components of the bulk velocity

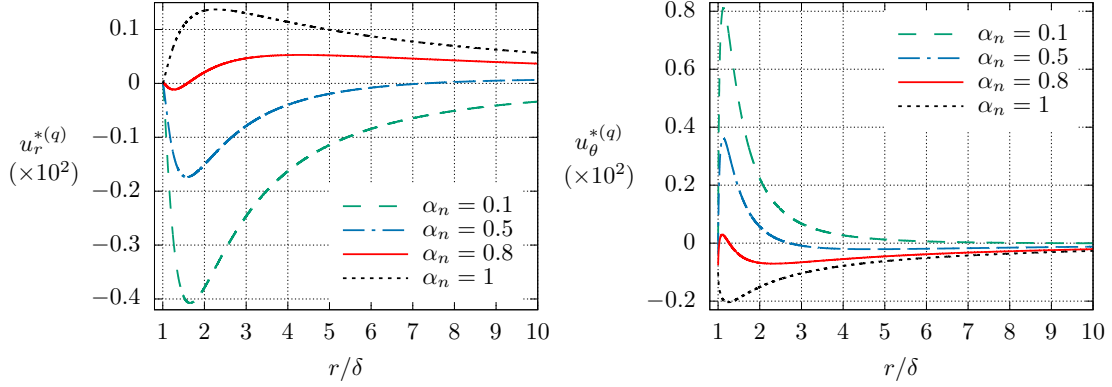


(b) Radial and polar components of the heat flux

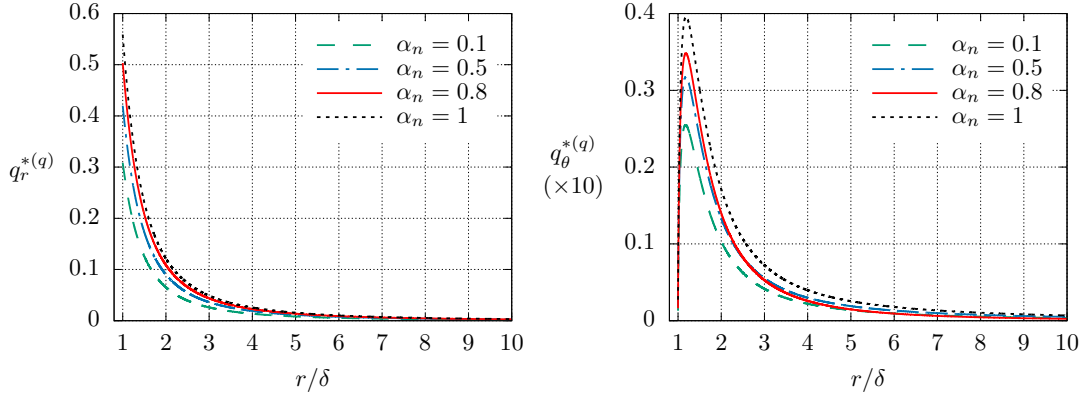


(c) Density and temperature deviations from equilibrium

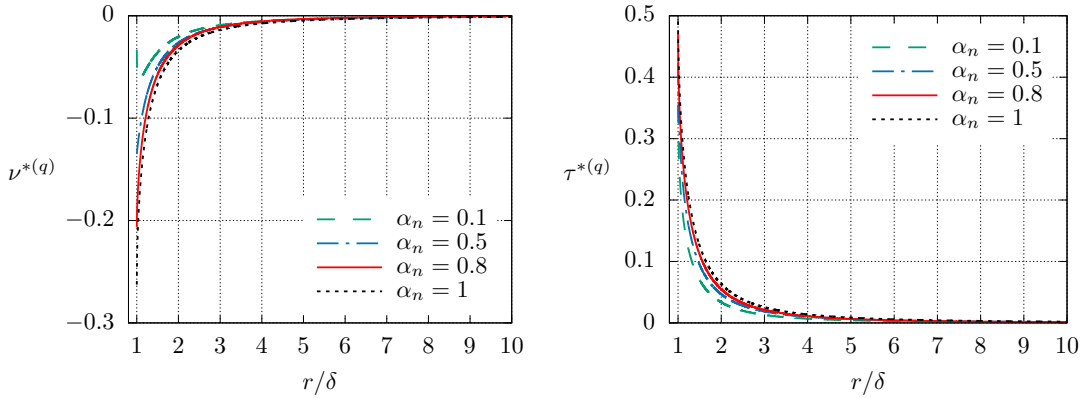
Figure 6: Flow fields due to the thermodynamic force X_q for fixed $\alpha_n=1$ and $\delta=0.1$.



(a) Radial and polar components of the bulk velocity

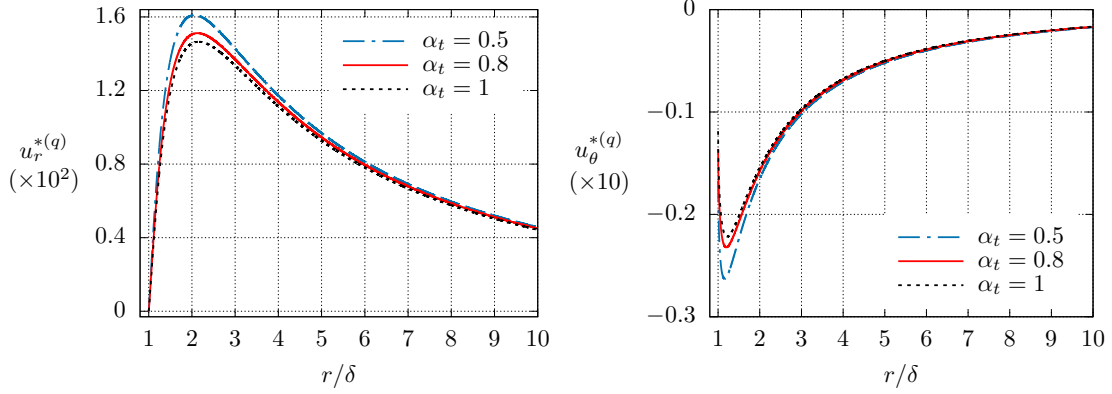


(b) Radial and polar components of the heat flux

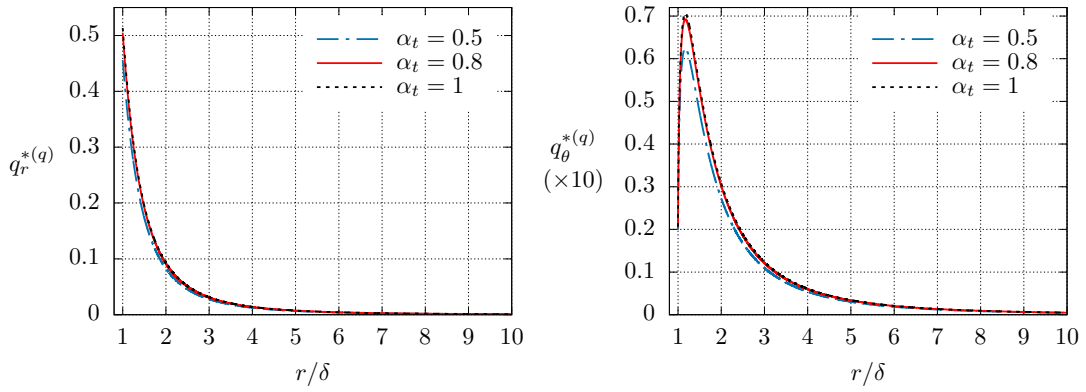


(c) Density and temperature deviations from equilibrium

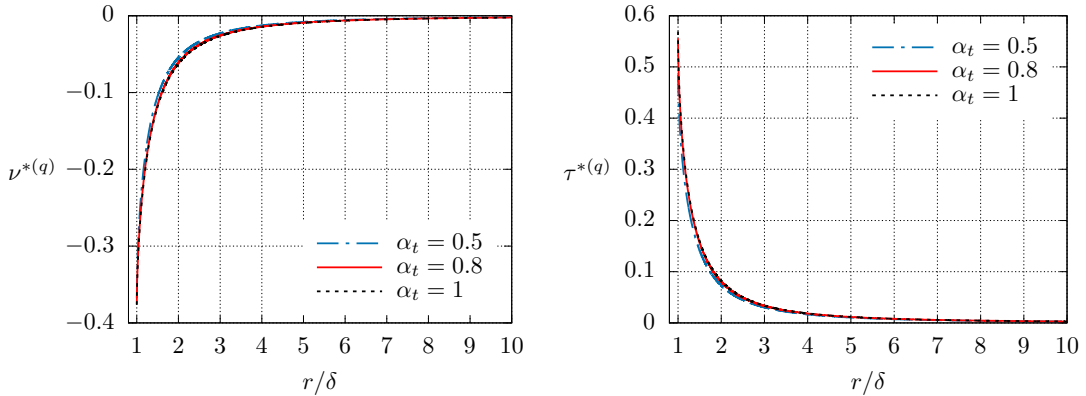
Figure 7: Flow fields due to the thermodynamic force X_q for fixed $\alpha_t=1$ and $\delta=0.1$.



(a) Radial and polar components of the bulk velocity

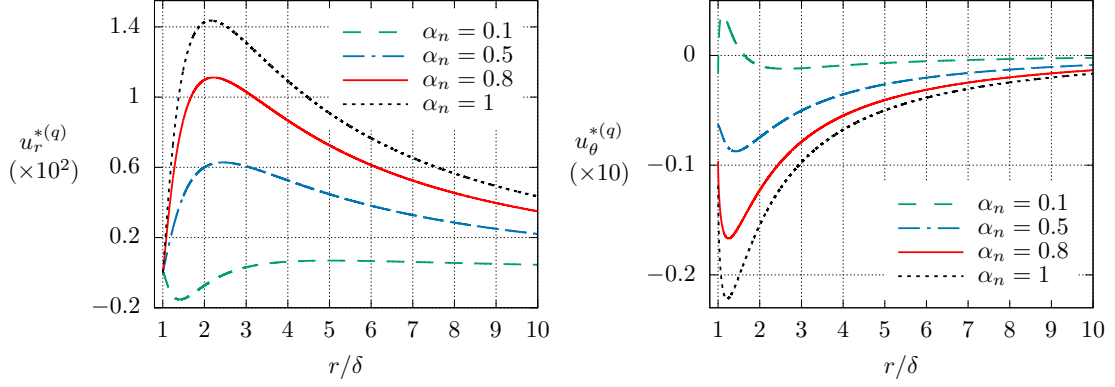


(b) Radial and polar components of the heat flux

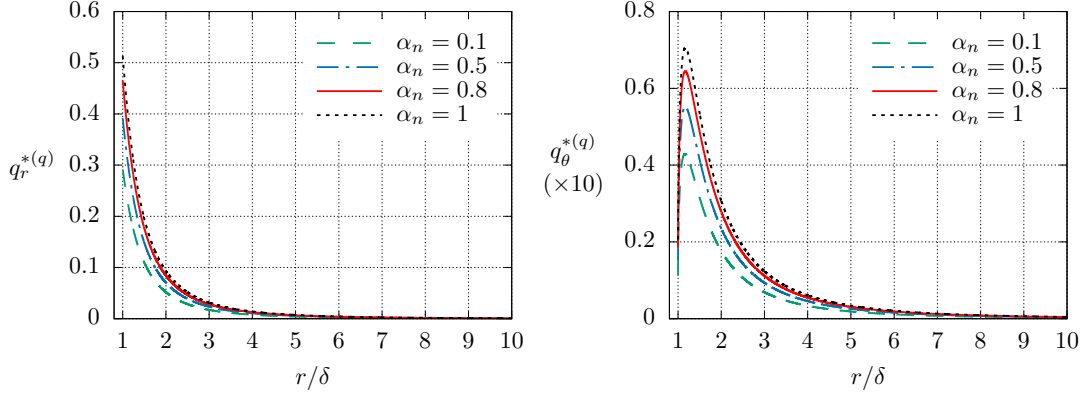


(c) Density and temperature deviations from equilibrium

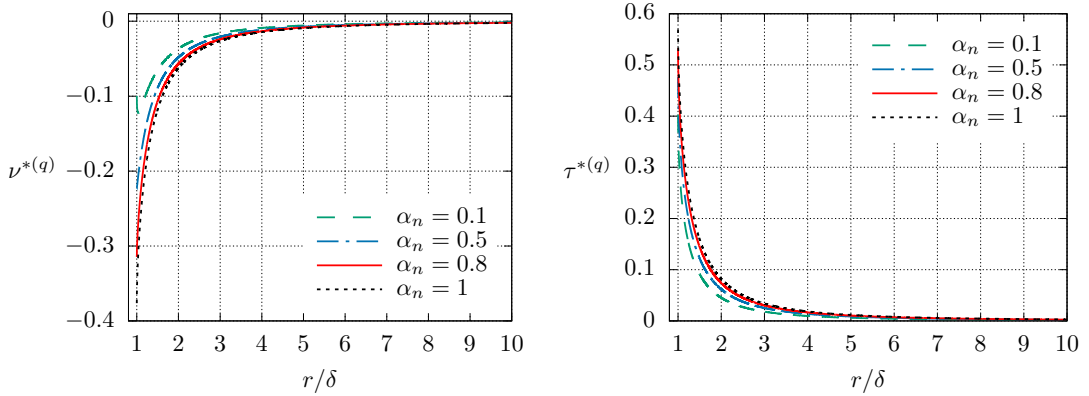
Figure 8: Flow fields due to the thermodynamic force X_q for fixed $\alpha_n=1$ and $\delta=1$.



(a) Radial and polar components of the bulk velocity

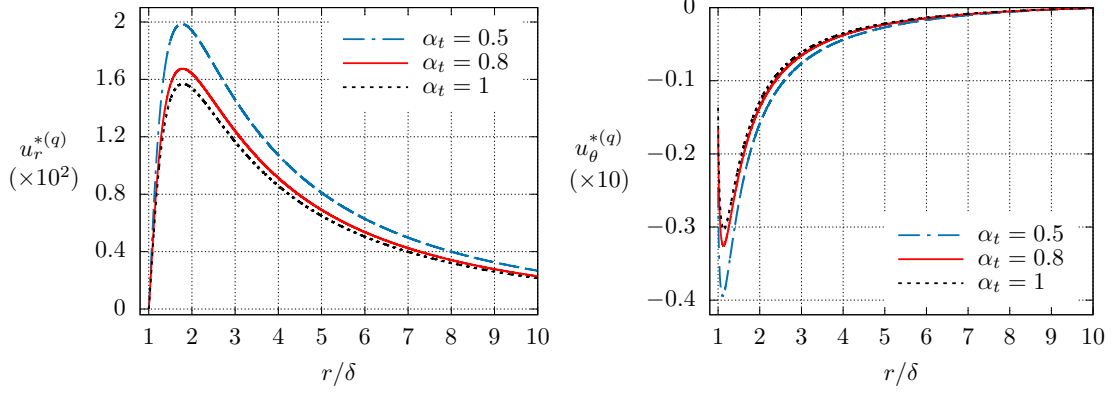


(b) Radial and polar components of the heat flux

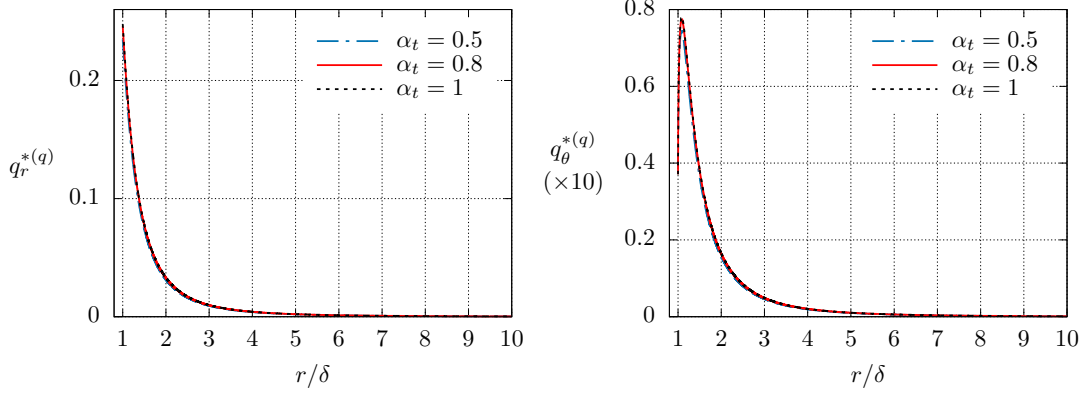


(c) Density and temperature deviations from equilibrium

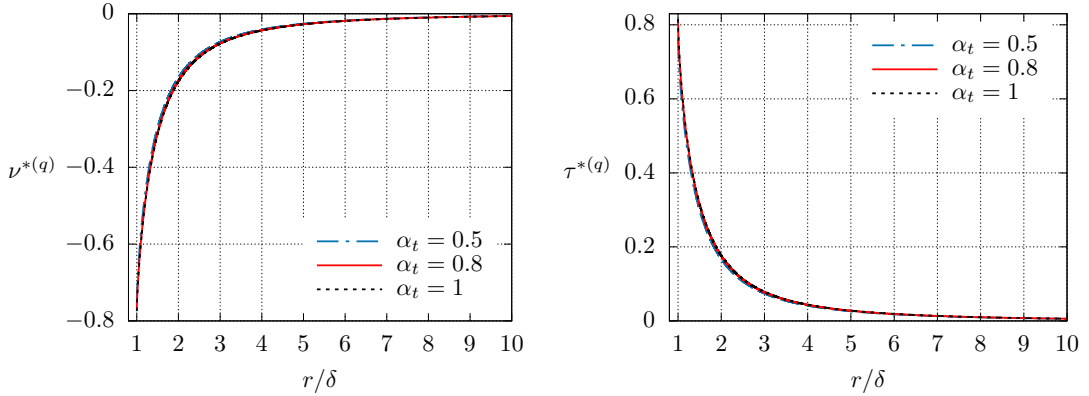
Figure 9: Flow fields due to the thermodynamic force X_q for fixed $\alpha_t=1$ and $\delta=1$.



(a) Radial and polar components of the bulk velocity

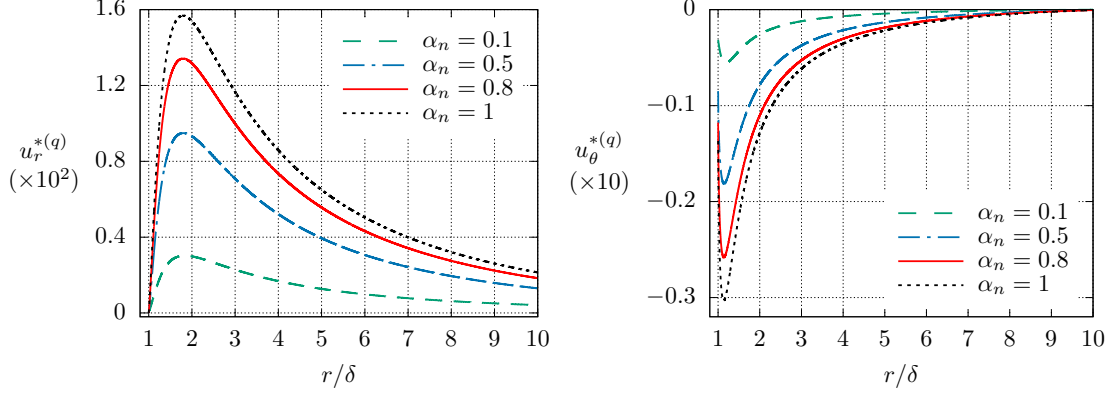


(b) Radial and polar components of the heat flux

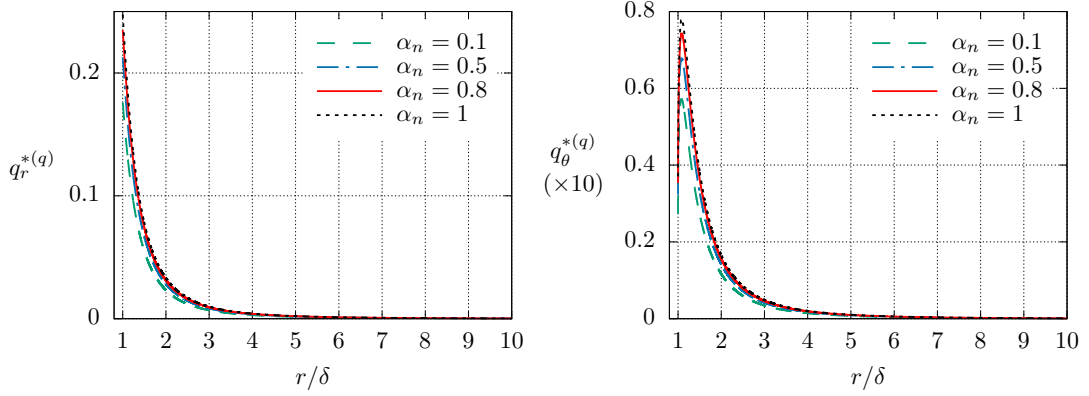


(c) Density and temperature deviations from equilibrium

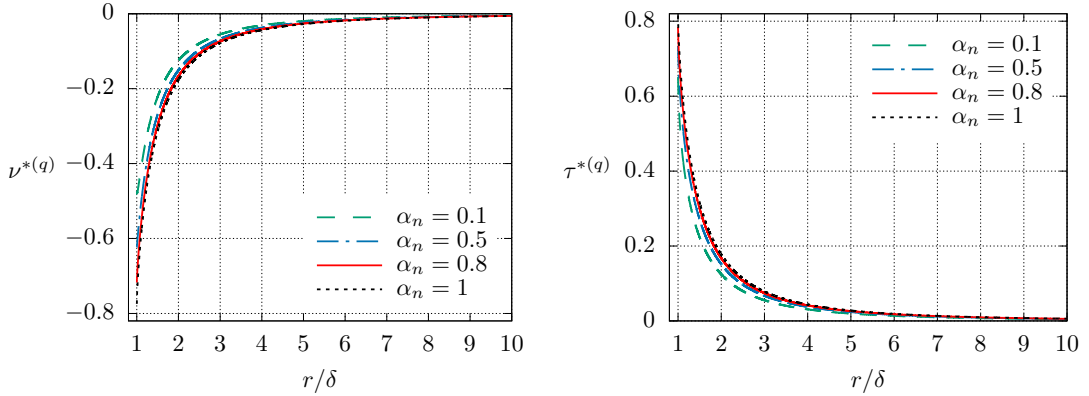
Figure 10: Flow fields due to the thermodynamic force X_q for fixed $\alpha_n=1$ and $\delta=10$.



(a) Radial and polar components of the bulk velocity



(b) Radial and polar components of the heat flux



(c) Density and temperature deviations from equilibrium

Figure 11: Flow fields due to the thermodynamic force X_q for fixed $\alpha_t=1$ and $\delta=10$.

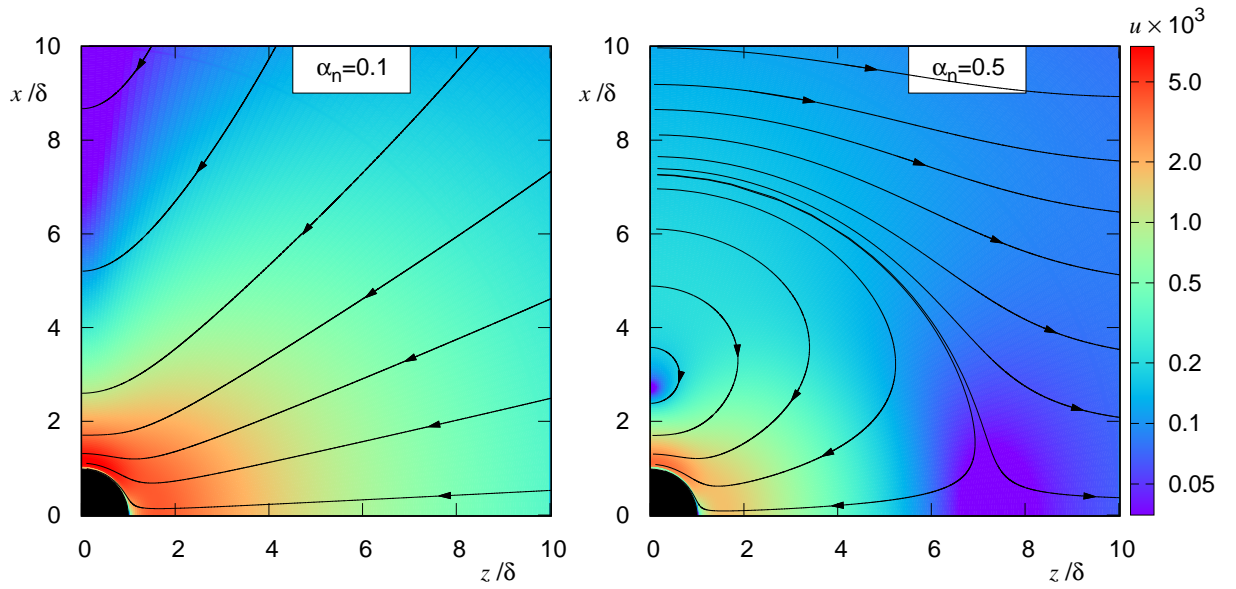


Figure 12: Speed contour and velocity streamlines for fixed $\alpha_t = 1$ and $\delta=0.1$.

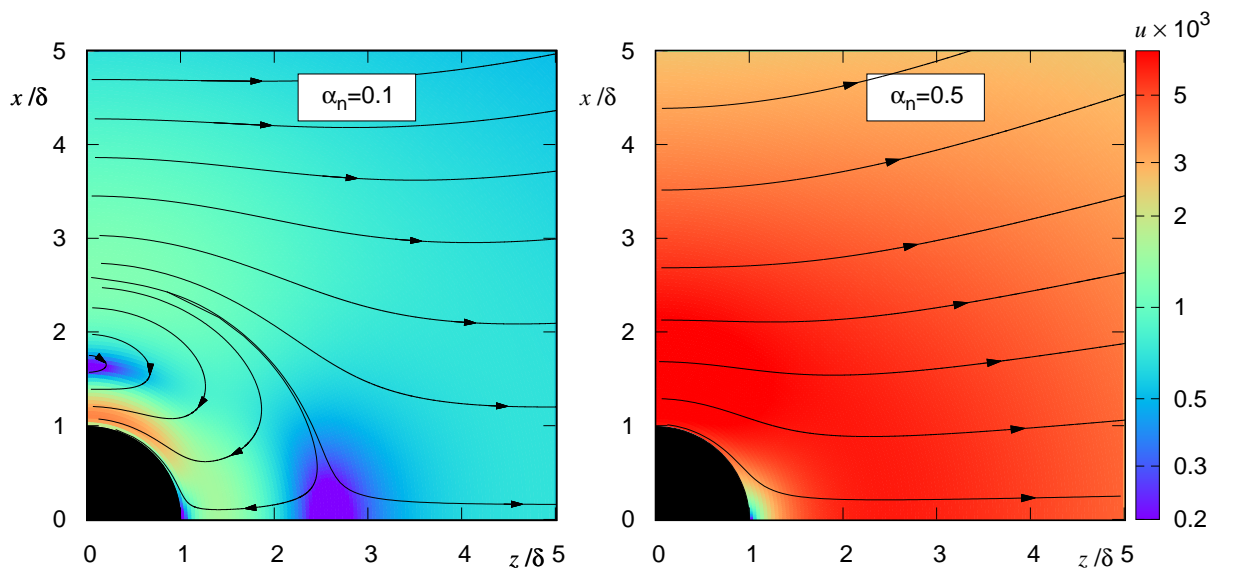


Figure 13: Speed contour and velocity streamlines for fixed $\alpha_t = 1$ and $\delta=1$.

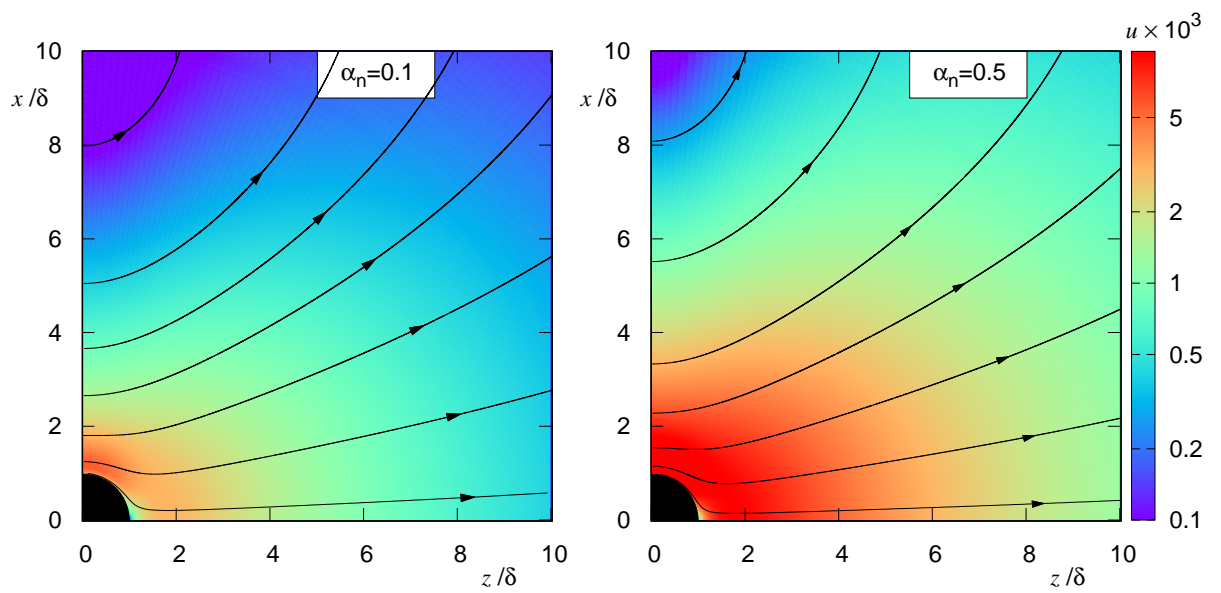


Figure 14: Speed contour and velocity streamlines for fixed $\alpha_t = 1$ and $\delta = 10$.

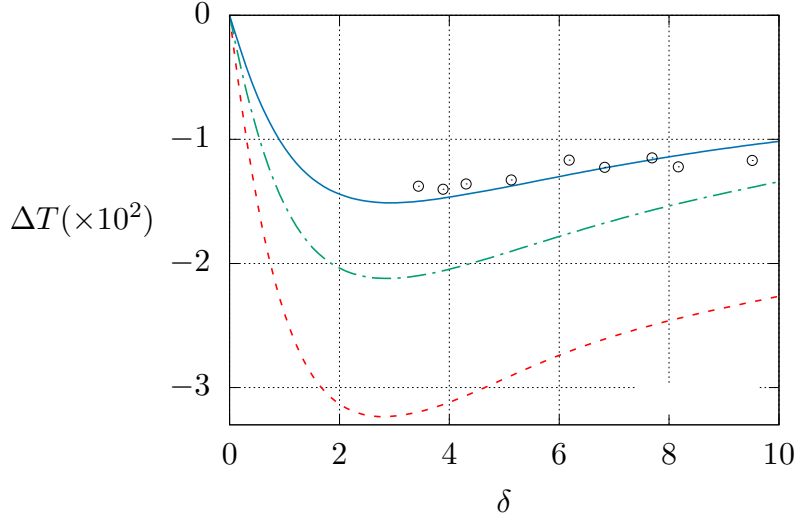


Figure 15: Temperature drop for helium gas at a Pyrex glass sphere ($\Lambda=7.5$) as function of the rarefaction parameter. Red dashed line: $\alpha_n=1$ and $\alpha_t=1$. Blue solid line: $\alpha_n=0.4$ and $\alpha_t=0.9$. Green interrupted line: $\alpha_n=0.6$ and $\alpha_t=0.9$. Symbol \odot : experimental data from Ref. [6].

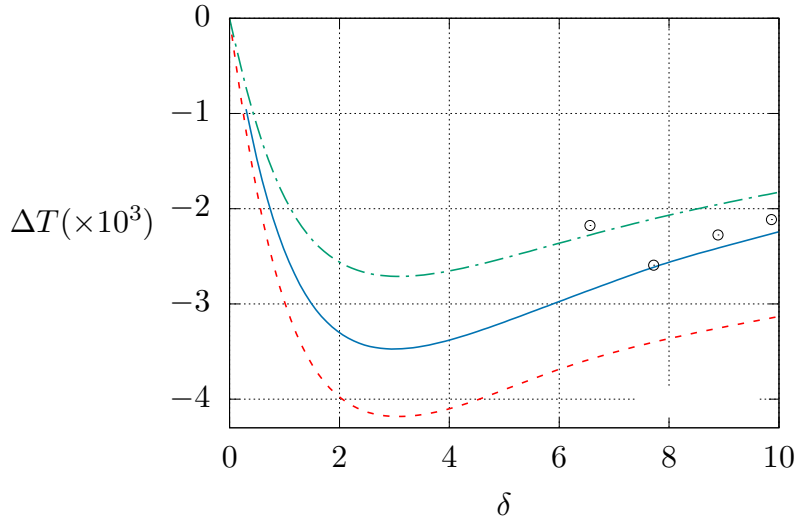


Figure 16: Temperature drop for argon gas at a Pyrex glass sphere ($\Lambda=62.5$) as function of the rarefaction parameter. Red dashed line: $\alpha_n=1$ and $\alpha_t=1$. Blue solid line: $\alpha_n=0.8$ and $\alpha_t=0.9$. Green interrupted line: $\alpha_n=0.6$ and $\alpha_t=0.9$. Symbol \odot : experimental data from Ref. [6].